AD NUMBER

AD849532

NEW LIMITATION CHANGE

TO

Approved for public release, distribution unlimited

FROM

Distribution authorized to U.S. Gov't. agencies and their contractors; Administrative/Operational Use; 01 NOV 1968. Other requests shall be referred to Naval Weapons Center, China Lake, CA.

AUTHORITY

USNWC ltr, 24 Mar 1972

HEAT TRANSFER IN SHOCK WAVE-BOUNDARY LAYER INTERACTION REGIONS

by

C. Franklyn Markarian
Weapons Development Department

ABSTRACT. An investigation of the effect of shock wave-boundary layer interaction on aerodynamic heat-transfer coefficients is reported. A literature survey and empirical expressions for predicting peak heat-transfer coefficients in interaction regions, developed with the use of existing experimental data, are presented.

NAVAL WEAPONS CENTER
CHINA LAKE, CALIFORNIA * NOVEMBER 1968

NAVAL WEAPONS CENTER
AN ACTIVITY OF THE NAVAL MATERIAL COMMAND

M. R. Etheridge, Capt., USN . . . . . Commander
Thomas S. Amtie, Ph.D. . . . . Technical Director

FOREWORD

A study of aerodynamic heating in regions of shock wave-boundary layer interaction is described in this report. The study was performed as part of the Aircraft-Missile Interference Effects Program, the purpose of which is to investigate the effect of the carrying aircraft on the flow field and of aerodynamic heating of airborne ordnance. Results of this study were originally published as a thesis submitted in partial fulfillment of the requirements for the degree Master of Science in Engineering at the University of California at Los Angeles.

This work was performed at the Naval Weapons Center, China Lake, Calif. during fiscal years 1967 and 1968. The project was funded by the Naval Air Systems Command under AirTask AIR-320-039/216-1/F009-10-01, Problem Assignment No. 3.

Technical review of this study was made by Bertha M. Ryan, of the Weapons Development Department, and by Robert H. Nunn, of the Propulsion Development Department. This report is released at the working level for information only.

Released by
R. W. VAN AKEN, Head,
Aeromechanics Div.
1 November 1968

Under authority of
F. H. KNEMEYER, Head,
Weapons Development Department

NWC Technical Publication 4485

Published by ..... Weapons Development Department
Manuscript 40/MS 67-73
Collation ..... Cover, 43 leaves, DD Form 1473, abstract cards
First printing ..... 170 unnumbered copies
Security classification ..... UNCLASSIFIED

CONTENTS

Figures:

ACKNOWLEDGMENT

The author wishes to express his appreciation to V. E. Denny, of the University of California at Los Angeles, for his help and guidance, and to R. D. Ulrich, formerly of the Propulsion Development Department, for suggesting the topic and providing valuable advice throughout the project.

NOTATION

b	Skin thickness
C_p	Pressure coefficient
C_f	Local skin-friction coefficient
c_p	Specific heat at constant pressure
F_1, F_2, F_3	Conical flow parameters (p. 62)
G_1, G_2, G_3	Conical flow parameters (p. 61)
h	Heat-transfer coefficient
k	Thermal conductivity
K_1, K_2	Experimental constants (p. 20)
K_L, K_T	Plateau pressure constants
ℓ_{SEP}	Separation length
M	Mach number
P	Pressure
Pr	Prandtl number, $\frac{c_p \mu}{k}$
q	Heat flux
Re_x	Reynolds number based on distance, $\frac{\rho V x}{\mu}$
Re_ζ	Reynolds number based on boundary-layer thickness, $\frac{\rho V \delta}{\mu}$
r	Recovery factor
St	Stanton number, $\frac{h}{\rho c_p V}$
T	Absolute temperature
t	Time

V	Velocity
x	Distance measured parallel to surface
x_{REF}	Reference distance defined in Fig. 10
y	Distance measured normal to surface
β	Shock angle
γ	Ratio of specific heats
δ	Boundary-layer thickness
θ	Flow-deflection angle
θ'	Separation angle
θ''	Reattachment angle
μ	Absolute viscosity
ξ	Pressure ratio (Appendix)
ρ	Density

Subscripts

0	Beginning of pressure rise
1	Immediately upstream of interaction
2	Shock impingement, immediately behind impinging shock; compression corner (no separation), behind compression shock; compression corner (separation), behind separation shock; fin shock, behind fin shock
3	Shock impingement (no separation), behind reflected shock; shock impingement (separation), behind reattachment shock; compression corner (separation), behind reattachment shock
AW	Adiabatic wall
d	Downstream of interaction
e	Boundary-layer edge

F	Final
FP	Flat plate
IW	Inner wall
LAM	Laminar boundary layer
OW	Outer wall
PK	Peak
PL	Plateau
R	Recovery
S	Surface
T	Total
TURB	Turbulent boundary layer
u	Upstream of interaction
W	Wall
∞	Free stream

Section 1
INTRODUCTION

BACKGROUND AND OBJECTIVES

The problem of aerodynamic heating, which has developed with the advent of supersonic flight, can be compounded considerably by various factors affecting the flow field. One of the most prominent of these factors is shock wave-boundary layer interaction. In addition to causing order-of-magnitude increases in the local aerodynamic heating rate, shock wave-boundary layer interaction alters the pressure distribution over a body and may cause boundary-layer separation. Shock wave-boundary layer interaction will occur on any vehicle with control surfaces, or other surface protuberances during supersonic and hypersonic flight.

Extensive work, both analytical and experimental, has been performed in the study of shock wave-boundary layer interaction. Most of the early work was concentrated on the pressure distribution in interaction regions; however, more recent studies have investigated the heat-transfer aspects of the problem. As the first phase of this study, a literature survey was made to determine (1) the current state-of-the-art of analytical solutions to the problem, and (2) the extent and findings of experimental investigations. Results of this survey are presented in Section 3. An extensive reference list, an author index, and a bibliography, giving related reports that were not used in this study, are included in this report.

Because the nature of the flow field in shock wave-boundary layer interaction regions is extremely complex, the analytical treatment of the problem presents a great deal of difficulty. A few successful methods of solution for laminar boundary-layer interaction have been developed but are quite involved. No analytical solutions for turbulent interactions are known to exist. The major difficulty in obtaining satisfactory analytical solutions has been in accurately describing the velocity and enthalpy profiles in the interaction region, particularly in cases in which separation occurs. Some of the more successful approaches to the problem are reviewed in Section 3.

Because there are complexities involved in analytical methods, a need exists for a rapid engineering method for estimating heat transfer in shock-interaction regions. Several empirical relations have been previously developed from the results of various experimental investigations; however, most of these were for specific configurations and were based on a limited amount of data. The objective of this study is to correlate as much of the existing experimental data as possible to determine the feasibility of developing general engineering methods for calculating heat transfer in shock wave-boundary layer interaction regions.

TYPES OF SHOCK WAVE-BOUNDARY LAYER INTERACTIONS

There are several manners in which shock wave-boundary layer interaction may arise. The following three types of interactions are treated in this study:

1. Planar shock wave, generated externally, impinging on and reflecting from a flat plate or cylinder.

2. Planar or conical shock wave generated within a boundary layer by a compression corner.

3. Planar shock wave generated by the leading edge of a fin mounted on a flat plate interacting with the boundary layer of the plate.

Two examples of the impinging-shock interaction are shown in Fig. 1. Figure 1(a) indicates a shock wave generated by the leading edge of an aircraft wing impinging upon a captive-flight missile. Other sources of impinging shock waves could be the aircraft air inlet, the missile launcher assembly, or additional underwing ordnance.

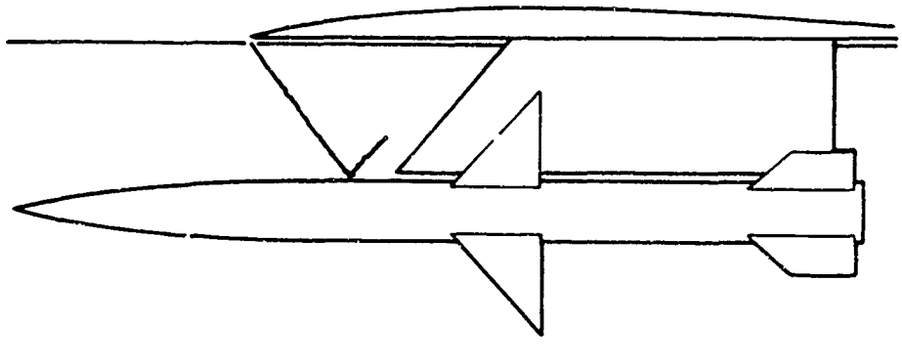

(a)

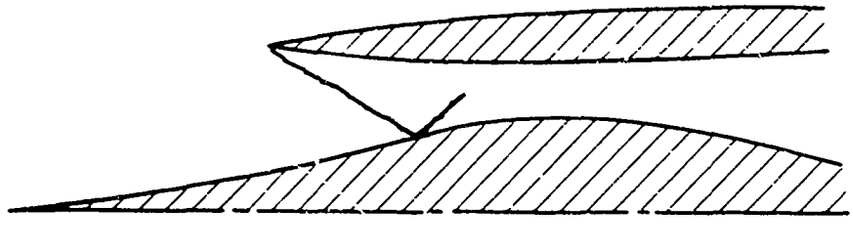

(b)

FIG. 1. Impinging-Shock Interaction on (a) a Captive-Flight Missile, and (b) an Inlet Diffuser.

As part of a study to investigate flow-interference effects in captive flight, this Center (NWC) has constructed and is flight testing an instrumented store of typical airborne configuration (Ref. 1). The round is currently instrumented to measure surface pressure, and it has been used to obtain pressure distributions at speeds up to Mach 1.9. Pressure distributions from supersonic flights have indicated the presence of impinging shock waves generated by the launcher assembly. With the use of the results, developed later in this report, the measured pressure rises in the shock-impingement regions correspond in some cases to increases in heat-transfer coefficient of over 100%. Increased heating rates and thermal gradients in the interaction regions could create serious aerodynamic heating problems, particularly if shock impingement occurred in the vicinity of the missile motor or warhead. Altered pressure distributions in the shock-interaction regions could also have an effect on separation of the store from the aircraft.

A problem which will exist in hypersonic air-breathing propulsion systems such as supersonic combustion ramjets (Scramjets) is shown in Fig. 1(b). This sketch illustrates the impingement upon the inlet diffuser of a shock wave generated by the lip of the air inlet.

Configurations which would cause compression corner interactions are a deflected flap, such as shown in Fig. 2, or a body with a conical flare.

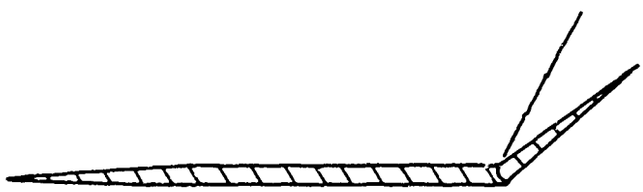

FIG. 2. Compression-Corner Interaction Generated by a Deflected Flap.

The type of interaction shown in Fig. 3 is present on any body with wings or fins while in supersonic flight. The leading edge of the fin generates a planar shock wave which interacts with the boundary layer on the surface of the body.

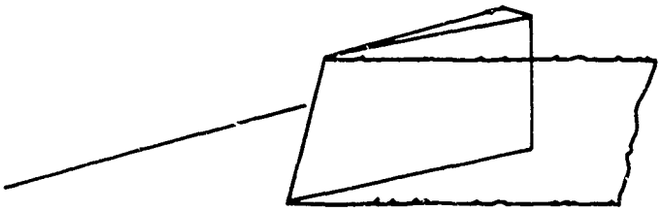

FIG. 3. Fin-Shock-Generated Interaction.

Other types of shock wave-boundary layer interactions, not treated in this study, are shown in Fig. 4, 5, and 6. Figure 4 shows an interaction caused by a surface protuberance, in this case a forward-facing step. The upstream portion of this type of interaction is similar to that of the previous types mentioned. This is an example of the free-interaction concept, which states that the upstream portion of the interaction region is independent of the source of the disturbance. Several analytical and experimental investigations of this type of interaction have been made (Ref. 2, 3, 4, 5, 6, 7, and 8). The shock-on-shock interaction (Ref. 9, 10, and 11) is illustrated in Fig. 5. This is a special case of the shock-impingement interaction in which an externally generated shock wave impinges on a surface that has a leading-edge shock. The externally generated shock interacts with the leading-edge shock before impinging on the boundary layer. An interaction of this type would result from a nose-generated bow shock impinging on the leading edge of a wing or fin. Hypersonic boundary-layer interaction (Ref. 12 and 13), shown in Fig. 6, arises when the shock wave generated at the leading edge of a surface is at a small enough angle to interact with the boundary layer.

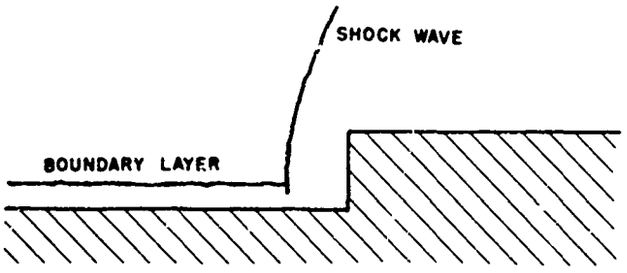

FIG. 4. Shock Wave-Boundary Layer Interaction Generated by a Forward-Facing Step.

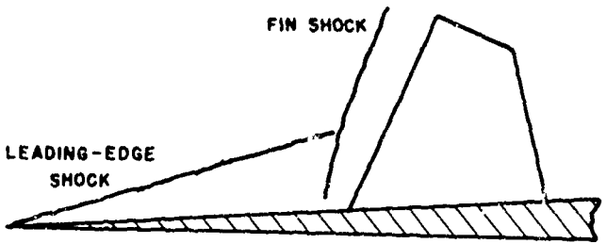

FIG. 5. Shock-On-Shock Interaction.

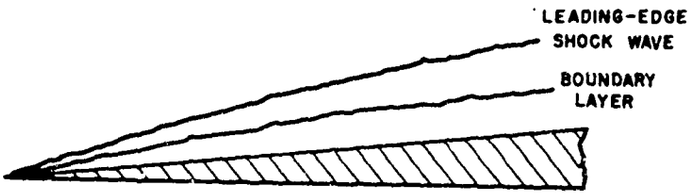

FIG. 6. Hypersonic Shock Wave-Boundary Layer Interaction.

Section 2

INTERACTION-REGION FLOW PATTERN

SHOCK IMPINGEMENT

The basic features of the shock-interaction region for the case of a planar shock wave impinging and reflecting from a laminar boundary layer are shown in Fig. 7. The pressure rise induced by the incident shock wave is propagated upstream through the subsonic portion of the boundary layer. As a result, the boundary layer thickens, and its momentum decreases. If the adverse pressure gradient is great enough, the skin friction will be reduced to zero and the boundary layer will separate. The region of separated flow is defined by the dividing streamline. Flow reversal takes place below the zero velocity streamline, as indicated by the velocity profile (Fig. 7). Streamline curvature away from the surface in the region of the thickening boundary layer creates a series of compression waves that merge to form a reflected shock wave, sometimes referred to as the separation shock. The incident shock is reflected from the constant-pressure separated region as a Prandtl-Meyer expansion fan. Upon passing through the incident shock and expansion fan, the flow is turned back toward the surface. As the flow reattaches and turns parallel to the plate, a second reflected shock, termed the reattachment shock, is formed. Immediately downstream of reattachment, the boundary-layer thickness reaches a minimum. It is in this region that the maximum heating rates occur.

In the case of shock impingement on a turbulent boundary layer, the length of the interaction region is considerably shorter than that of the laminar boundary layer. This results because a turbulent boundary layer has greater momentum than has a laminar boundary layer, and it can more successfully sustain an adverse pressure gradient. As a result, a much greater pressure rise is required to cause separation of a turbulent boundary layer than separation of a laminar boundary layer.

COMPRESSION CORNER

The flow field corresponding to a compression-corner interaction is shown in Fig. 8. As in the case of the impinging-shock interaction, the pressure disturbance, this time generated by the compression corner, propagates upstream through the subsonic portion of the boundary layer. In the process, the boundary layer thickens; a compression shock is formed; and if the pressure gradient is large enough, boundary-layer separation occurs. If the turning angle is large enough, the compression will take place in two phases (Fig. 8). In the first phase,

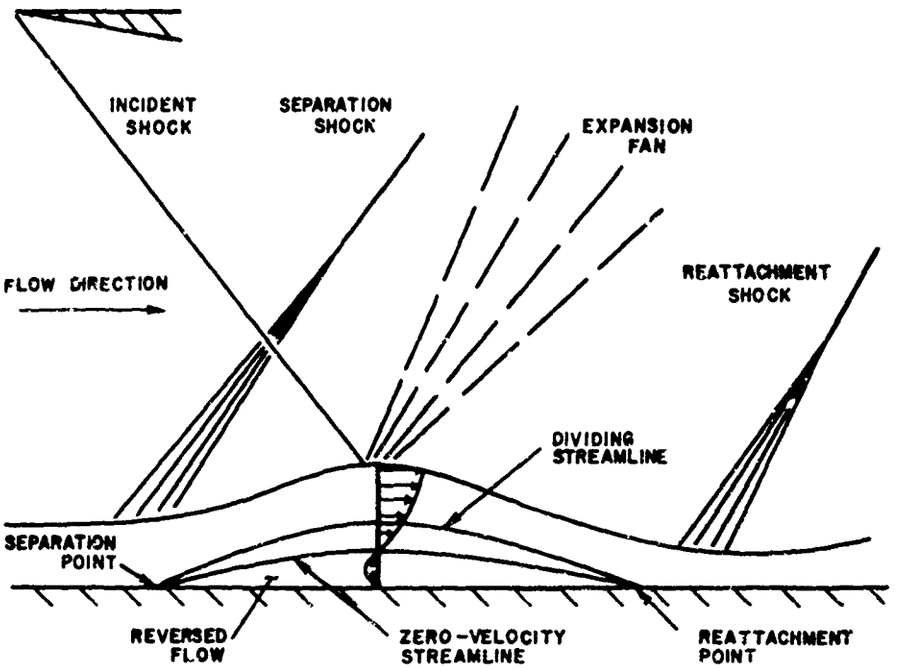

FIG. 7. Schematic Representation of an Oblique Shock Wave Impinging on a Laminar Boundary Layer.

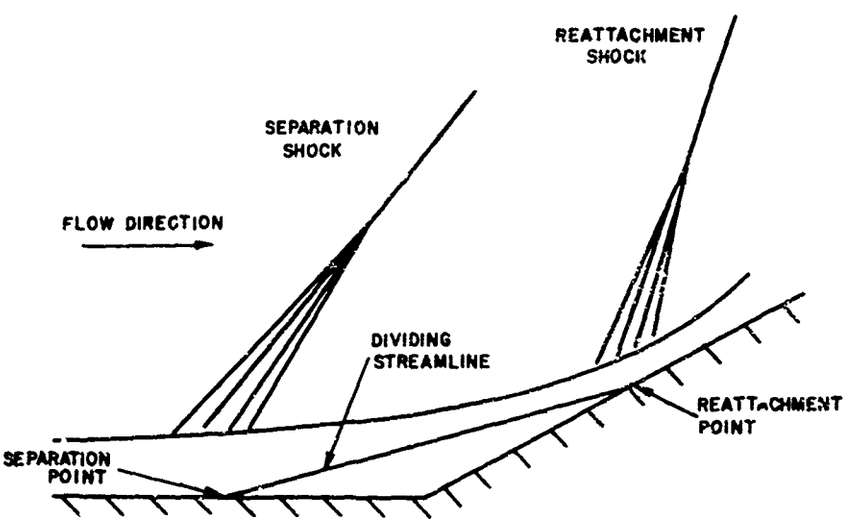

FIG. 8. Schematic Representation of a Compression-Corner-Generated Interaction.

a separation shock is formed as a result of streamline curvature caused by separation; in the second phase, a reattachment shock is formed as the flow turns parallel to the compression surface. Experiments show that pressure and heat-transfer distributions are quite similar for the impinging shock and compression-corner interactions.

FIN-GENERATED SHOCK WAVE

The flow field associated with the interaction between the shock wave generated by the leading edge of an unswept fin and a boundary layer is considerably more complicated than the two cases discussed previously. This arises from the fact that the sweep of the fin shock creates a three-dimensional rather than a two-dimensional interaction. If, however, the flow field is viewed in a plane normal to the direction of the shock wave (Fig. 9), the flow field appears similar to that of a two-dimensional interaction. Although the lambda-shock configuration differs from the previous interactions, the separation shock, expansion fan, and reattachment shock are still present. Pressure and heat-transfer distributions take the same form as those in the impinging-shock and compression-corner interactions. Leading-edge sweep alters these distributions, but the general trend remains the same.

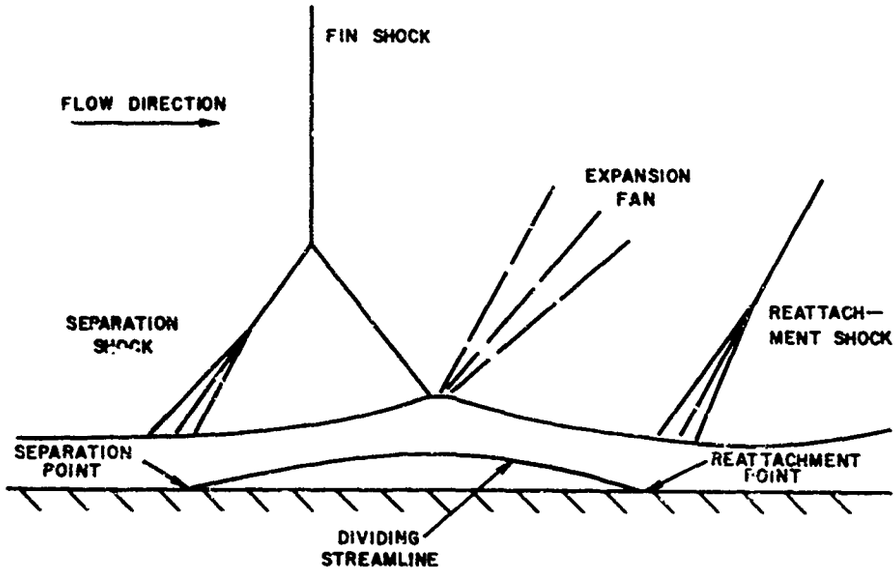

FIG. 9. Schematic Representation of a Fin-Shock-Generated Interaction.

PARAMETERS REQUIRED TO DESCRIBE INTERACTION

To adequately describe the interaction, the follcwing conditions and parameters must be determined.

1. Type of boundary layer

   a. Laminar (transition downstream of interaction); turbulent (transition upstream of interaction); or transitional (transition within interaction region)

   b. Attached or separated

2. Interaction geometry

   a. Location and length of interaction region

   b. Separation and reattachment points

3. Pressure distribution (primarily peak pressure and in separated regions, plateau pressure)

4. Heat-transfer distribution (primarily peak heat transfer and heat transfer in separated region)

Section 3
LITERATURE SEARCH

ANALYTICAL STUDIES

Because the nature of shock wave-boundary layer interactions is complex, attempts at analytical solutions to the problem have achieved only limited success. The successful approaches are limited to the case of two-dimensional or axisymmetric laminar boundary layers; although some semiempirical work has been performed on turbulent interactions (Ref. 14). Almost all of the approaches utilize momentum integral methods. The flow is described by solving the boundary-layer equations governing conservation of mass, momentum, and, if the flow is nonadiabatic, energy. The primary difficulty in solving the boundary-layer equations is in specifying velocity and enthalpy profiles that accurately describe the flow reversal which takes place in separated regions.

Several of the earlier studies (Ref. 15, 16, and 17) utilized the Karman-Pohlhausen momentum-integral method, in which the velocity profile is related to the local static-pressure gradient. Some success was achieved by Martellucci and Libby (Ref. 17), who used this method with quartic velocity profiles. These approaches, however, did not adequately describe conditions within separated regions.

Improved solutions were obtained with a semiempirical method developed by Crocco and Lees (Ref. 18) and modified by Glick (Ref. 19), in which the velocity profile was not directly related to the local static-pressure gradient. The semiempirical features of the Crocco-Lees method were eliminated by Tani (Ref. 20) in a method which, in addition to the aforementioned boundary-layer equations, utilized the moment of momentum equation. This approach, termed the two-moment method, gave good agreement with experimental data except in separated regions. Difficulties were encountered in these regions because of the use of quartic velocity profiles. Lees and Reeves (Ref. 21) demonstrated that polynomial velocity profiles described by a single parameter do not exhibit the correct behavior in separated flows. The velocity profiles in a separated region can be more accurately described by polynomial expressions with two or more parameters, or by representing the velocity profiles above and below the zero velocity streamline (Fig. 7) by a different family of profiles. Lees and Reeves used the later approach, obtaining the velocity and enthalpy profiles for attached and separated flows by using the upper and lower branch solutions, respectively, of the compressible flow analogs to the Falkner-Skan equations. Good agreement was achieved with experimental data for interactions on an adiabatic wall. In the case of of an adiabatic or moderately cooled wall, the enthalpy profiles may be

linked to the velocity profiles, as was done by Lees and Reeves. However, in the case of a highly cooled wall, the enthalpy profile must be specified independently by use of the energy equation. This was done by Holden (Ref. 22), who used a slightly modified Lees and Reeves (Ref. 21) approach. Excellent agreement was obtained with experimental data obtained from interactions on highly cooled walls.

Successful solutions to the shock-interaction problem were also developed by Makofski (Ref. 23) and Nielsen (Ref. 24). Makofski obtained a solution for laminar interactions on an adiabatic wall by representing the velocity profile by a fifth-degree polynomial with two undetermined parameters. Nielsen developed methods for laminar flow over both adiabatic and nonadiabatic walls.

EXPERIMENTAL INVESTIGATIONS

A number of experimental investigations have been made of shock wave-boundary layer interactions. Most of the early work, such as the studies of Chapman, Kuehn, and Larson (Ref. 25), and Hakkinen and others (Ref. 26), was concerned with the effects of the interaction on pressure and skin-friction distributions and boundary-layer separation. In more recent studies, measurements of the heat-transfer distributions through interaction regions have been made. This report correlates the results of the heat-transfer investigations in order to obtain empirical means for predicting the maximum heat transfer and the heat-transfer distribution in shock wave-boundary layer interaction regions. Results of the experimental investigations described herein are used in these correlations. The test parameters for these investigations are summarized in Table 1.

Levin and Fabish

The thermal effects of shock-wave impingement on a turbulent boundary layer were investigated in a study conducted by Levin and Fabish (Ref. 27). Tests were conducted in a wind tunnel at free-stream Mach numbers of 2.95 and 5.02 and Reynolds numbers per foot of 7.4×10^6 and 3.6×10^6, respectively. The boundary layer was generated by a sharp leading-edge flat plate instrumented to measure pressure and heating rates. Boundary-layer velocity profiles were measured upstream and downstream of the interaction. Turbulent flow upstream of the interaction region was assured by means of boundary-layer air injection and grit. Air injection was also used to investigate the effects of upstream thickening of the boundary layer. The oblique shock-wave generator was varied in attitude from 0 to 12 degrees and was adjusted so that shock impingement occurred approximately 11.75 inches from the leading edge of the flat plate. Runs were also made with the shock

TABLE 1. Summary of Test Parameters

Ref.	Type interaction	M_∞	θ, deg	Re_∞/ft x 10^{-6}	T_T, °R	P_T, psi	Boundary layer
27	Shock impingement on flat plate	2.95	6.0	7.4	573	50.0	Turbulent
		2.95	6.0	7.4	570	50.0	Turbulent
		2.95	9.5	7.4	570	49.8	Turbulent
		2.95	9.5	7.4	575	49.9	Turbulent
		2.95	12.0	7.4	573	48.6	Turbulent
		2.95	12.0	7.4	575	50.0	Turbulent
		2.95	12.0	7.4	570	50.6	Turbulent
		5.02	7.4	3.6	570	64.0	Turbulent
		5.02	9.7	3.6	565	63.8	Turbulent
		5.02	9.7	3.6	568	63.8	Turbulent
		5.02	11.0	3.6	565	64.0	Turbulent
		5.02	11.0	3.6	565	64.2	Turbulent
		5.02	11.0	3.6	566	63.9	Turbulent
		5.02	12.0	3.6	560	63.8	Turbulent
		5.02	12.0	3.6	568	63.7	Turbulent
28	Shock impingement on flat plate	2.41	8.0	4.74	580	24.8	Turbulent
		2.41	15.0	4.74	580	24.8	Turbulent
		3.01	8.0	4.53	565	31.2	Turbulent
		3.01	15.0	4.53	565	31.2	Turbulent
		3.01	26.0	4.53	565	31.2	Turbulent
		3.99	8.0	4.23	580	50.7	Turbulent
		3.99	15.0	4.23	580	50.7	Turbulent
		5.01	15.0	3.21	605	63.6	Turbulent
	Shock impingement on cylinder	2.41	8.0	4.66	591	24.8	Turbulent
		2.41	15.0	4.66	591	24.8	Turbulent
		3.01	8.0	4.30	579	30.8	Turbulent
		3.01	15.0	4.30	579	30.8	Turbulent
		3.99	8.0	4.18	587	50.1	Turbulent
		3.99	15.0	4.18	587	50.1	Turbulent
		5.01	8.0	2.33	583	46.2	Turbulent
		5.01	15.0	2.33	583	46.2	Turbulent
29	Shock impingement on flat plate	10.18	0	2.16	1,890	1,800	Turbulent
		10.18	5	2.16	1,890	1,800	Turbulent
		10.18	10	2.16	1,890	1,800	Turbulent
		9.98	10	0.5	1,735	335	Laminar
30	Compression corner (wedge)	8.13	9.5	2.06	1,334	459	Laminar
		8.12	15.0	1.89	1,336	420	Laminar
		8.07	13.9	1.42	1,265	292	Laminar
		8.02	9.4	0.99	1,248	197	Laminar
		8.12	18.5	1.85	1,383	437	Laminar
		9.7	10.0	1.53	1,344	522	Laminar
		9.7	13.7	1.50	1,375	534	Laminar
		9.68	10.0	1.31	1,346	446	Laminar
		9.7	18.0	1.46	1,355	508	Laminar
31	Compression corner (wedge)	9.7	7.6	1.8	...	...	Laminar
		9.7	10.0	1.8	...	...	Laminar
33	Compression corner (wedge)	2.495	15	13.25	563	108	Turbulent
		3.23	15	13.21	563	108	Turbulent
		3.59	15	11.83	563	108	Turbulent
		3.97	15	9.92	563	108	Turbulent
		4.36	15	8.33	563	108	Turbulent
34	Compression corner (conical flare)	6.8	10	1.52	1,100	47-630	Laminar
		6.8	10	5.6	1,100	47-630	Turbulent
		6.8	30	5.04	1,100	47-630	Turbulent
		6.8	30	1.12	1,100	47-630	Transition
35	Compression corner (conical flare)	4.98	10	1.6	710	...	Laminar
		4.98	10	5.4	710	...	Transition
		4.98	24	5.4	710	...	Transition
		4.98	24	5.4	710	...	Turbulent
		4.98	56	5.4	710	...	Turbulent
36	Fin shock	8	7.5	2.0	...	...	Laminar
		8	15.0	2.0	...	...	Laminar
37	Fin shock	16	0	0.2	5,800	8,000	Laminar
		16	5	0.2	5,800	8,000	Laminar
		16	7.5	0.2	5,800	8,000	Laminar
		16	15.0	0.2	5,800	8,000	Transition

generator removed. Heating rates on the flat plate were measured by the use of Nichrome ribbon heating elements that were maintained at a fixed temperature above the total temperature of the flow. The heating rate was obtained from the following relation:

$$q = \frac{\left(\begin{array}{c}\text{Power dissipated} \\ \text{by element}\end{array}\right) - \left(\begin{array}{c}\text{Power conducted} \\ \text{and radiated away} \\ \text{from element}\end{array}\right)}{\text{Planform area of element}}$$

Heat-transfer data was presented in the form of heat-transfer coefficient obtained from the equation

$$q = h \left(T_{element} - T_{AW}\right)$$

In some cases, shock impingement caused boundary layer separation. Peak heat transfer always occurred within the pressure interaction region and increased with increasing pressure rise. In the cases of separated flow, peak heat transfer occurred at reattachment. Air injection into the boundary layer upstream of the interaction did not significantly alter the heat-transfer distribution in the interaction region.

Sayano

In a study similar to that of Levin and Fabish (Ref. 27), Sayano (Ref. 28) investigated the effects of planar-shock impingement on flat plates and cylinders. Tests were conducted in a 20-inch wind tunnel. Pressure and heat-transfer data were obtained at free-stream Mach numbers of 2.41, 3.01, 3.99, and 5.01. Free-stream Reynolds number per foot ranged from 2.56×10^6 to 4.73×10^6. A boundary-layer trip assured turbulent flow upstream of the interaction. Runs were made with shock generator angles of 8, 15, and 26 degrees and with the shock generator removed. Shock impingement occurred approximately 20 inches from the leading edge of the flat plate and the nose of the cone-cylinder.

Heat-transfer measurements were made by cooling the back surface of the instrumented section and relating heat-transfer coefficient to the gradient across the wall of the section by the following expression:

$$h \left(T_R \quad T_{OW}\right) = \frac{k}{b} \left(T_{OW} - T_{IW}\right)$$

Radiation and conduction effects were neglected, and the accuracy of the measurements was estimated at 15%. Pressure and heat-transfer coefficient distributions were nondimensionalized by the distributions obtained with the shock generator removed.

Boundary-layer separation occurred with shock-generator angles of 15 and 26 degrees. The basic difference in shock-impingement effects between the flat plate and the cylindrical boundary layers was that the interaction region was considerably larger and the increase in pressure and heat-transfer coefficient was greater on the flat plate. This difference can be attributed to crossflow on the cylinder caused by the favorable circumferential pressure gradient.

Peak heat transfer occurred in the same vicinity as peak pressure for both the flat plate and cylindrical boundary layers. In all cases, the rise in heat-transfer coefficient in the interaction region increased with increasing shock strength.

Magnan and Spurlin

Planar-shock-impingement effects on laminar and turbulent flat-plate boundary layers were investigated by Magnan and Spurlin (Ref. 29). Tests were conducted in a 50-inch-diameter continuous-flow wind tunnel at a nominal free-stream Mach number of 10 and free-stream Reynolds numbers per foot of 0.5×10^6 and 2.16×10^6. The impinging shock wave was generated by a blunt leading-edge flat plate set at angles of incidence of 0, 5, and 10 degrees. The position of the shock generator was adjusted so that shock impingement occurred approximately 22 to 24 inches from the leading edge of the flat plate in the case of the turbulent boundary layer, and 12 inches in the case of the laminar boundary layer.

The flat plate was instrumented to measure both pressure and heating-rate distributions. Heating rates were measured by the transient thin-skin method. The test plate, instrumented with thermocouples, was cooled to room temperature between runs before being injected into the air stream. The heating rate was related to the measured temperature response by the expression.

$$q = \rho b c_p \frac{dT_W}{dt}$$

which neglects conduction and radiation effects. Heat-transfer coefficients were obtained from the expression

$$h = \frac{q}{(T_T - T_W)}$$

The reason for using total temperature rather than the more conventional recovery temperature in this expression was not given. If the heat-transfer coefficients of Ref. 29 are recalculated based on recovery temperature, the turbulent values are increased approximately 20%, and the laminar values approximately 25%. In the correlations, given in Section 5, the peak heat-transfer coefficients (as obtained from Ref. 29) are usually below the general trend of the data.

Boundary-layer separation occurred in the case of shock impingement on the laminar boundary layer. Peak heat-transfer coefficients occurred in the same region as peak pressures and increased with increasing shock strength. Some difficulty was encountered in accurately determining pressure and heat-transfer coefficients from the plots provided in the report, particularly the values upstream of the interaction.

Popinski

An experimental investigation of shock wave-laminar boundary layer interaction in a two-dimensional compression corner (ramp) was conducted by Popinski (Ref. 30). Tests were performed in a blow-down wind tunnel at nominal free-stream Mach numbers of 8 and 10 and Reynolds numbers per foot ranging from 1×10^6 to 2×10^6. For use in the correlations, Mach numbers immediately upstream of the interaction region were calculated by assuming an isentropic compression through a leading-edge Mach wave from the free-stream pressure to the measured pressure on the plate.

Pressure and heat-transfer measurements were made on a sharp leading-edge flat plate with an adjustable ramp that could be set at angles varying from 0 to 25 degrees. The corner was located 13.4 inches from the leading edge of the plate.

Heat-transfer coefficients were determined by the transient thin-skin method with corrections made for spanwise and transverse conduction. Radiation effects were neglected. The following relation was used:

$$h\left(T_{AW} - T_W\right) = bc_p \frac{dT_W}{dt} - bk\left(\frac{\partial^2 T_W}{\partial x^2} + \frac{\partial^2 T_W}{\partial y^2}\right)$$

The temperature response of the flat plate was measured by means of thermocouples. Average wall to total temperature ratio throughout the tests was approximately 0.4. Measured heat-transfer coefficients were nondimensionalized by the theoretical flat-plate value at the corner. The distribution of pressure taps did not allow the measurement of peak pressure on the ramp. For correlation purposes, the inviscid pressure ratio calculated from the upstream Mach number and ramp angle was used.

Boundary-layer separation occurred on most of the runs. This was indicated by a plateau in the pressure distribution and a decrease in heat-transfer coefficient below the flat-plate value in the vicinity of the corner. Peak heat-transfer coefficients occurred on the ramp and increased with increasing pressure rise. Peak heat transfer was observed to increase with decreasing free-stream Reynolds number.

Needham

Laminar interactions in a wedge-type compression corner were studied experimentally by Needham (Ref. 31). The object of the investigation was to determine if the heat-transfer distribution could be used as a criterion for detecting the onset of separation. Tests were conducted in a hypersonic gun tunnel at a freestream Mach number of 9.7 and Reynolds number per foot of 1.23×10^4. The local Mach number upstream of the corner was determined by Shumway (Ref. 32) to be approximately 8. Wedge angles were varied from 7.6 to 15.3 degrees; although, peak heat-transfer measurements were presented only for wedge angles of 7.6 and 10 degrees. The corner was located 6 inches from the leading edge of the model.

The model was instrumented to measure pressure and heat-transfer distributions. Heating rates were measured with thin-film resistance thermometer gages. Data were presented as pressure and heating rates nondimensionalized by flat-plate values. Heating rates were converted to heat-transfer coefficients by the method developed by Shumway. Boundary-layer separation occurred at wedge angles of 10 degrees and greater.

Hastings, and Others

Turbulent heat transfer in a wedge compression-corner was investigated by Hastings, Brown, and Atkinson (Ref. 33). Tests were conducted in a 3- by 4-foot wind tunnel at a free-stream Mach number of 4. Mach numbers upstream of the corner were varied from 2.5 to 4.4 by pitching the model. The corresponding free-stream Reynolds numbers per foot ranged from 13.25×10^6 to 8.33×10^6.

The model, instrumented to measure pressure and heating rates, consisted of a sharp leading-edge flat plate with a 15-degree wedge. The corner was located 7.25 inches from the leading edge of the plate. Steady-state heating rates, measured by heat flux gages, were obtained by cooling the test section of the model. Heat-transfer data was presented in the form of Stanton number which was obtained from the expression

$$St = \frac{q}{\rho V c_p (T_R - T_W)}$$

Stanton numbers on the ramp were referenced to conditions both upstream and downstream of the corner.

Boundary-layer separation was not observed during the testing. Although a significant increase in Stanton number occurred on the ramp, heating rates both upstream and downstream of the corner were lower than had been estimated. The authors were therefore uncertain as to the accuracy of the data. Heat-transfer instrumentation of the ramp did not appear dense enough to assure that the peak heating rate would be measured. Because of these factors, results of this study were used with caution in the present correlations.

Becker and Korycinski

Pressure and heat-transfer distributions in the vicinity of conical flare compression-corners were investigated in wind tunnel tests by Becker and Korycinski (Ref. 34). Laminar, turbulent, and transitional boundary layers were investigated at a free-stream Mach number of 6.8 and Reynolds numbers per foot from 1.12×10^7 to 5.6×10^7. The model consisted of an ogive-cylinder with conical flare skirts. Flare half-angles of 10 and 30 degrees were tested. The flare-cylinder junction was 15 inches (10 body diameters) from the nose of the model.

Separate models were used for pressure and heat-transfer measurements. Heating rates were determined by the transient thin-skin method. The model was cooled to room temperature before being injected into the airstream. Heat-transfer data were presented in terms of the Stanton number. Since the Stanton numbers were based on free-stream conditions, the Stanton number ratio was equal to the heat-transfer-coefficient ratio, which was used in the correlations developed in this report.

Boundary-layer separation occurred in the case of laminar interaction with a 10-degree flare. Heating rates in the separated region were approximately 50% of the theoretical attached value. The measured peak-heat transfer was below the value which was calculated by assuming that a new boundary layer started at the reattachment point. Peak heat transfer occurred downstream of reattachment.

In the turbulent case, a small separation region existed with the 30-degree flare, but not with the 10-degree flare.

Extensive separation occurred in the case of the transitional boundary layer with the 30-degree flare. Heating rates in the separated region were initially below the attached value, but increased rapidly following transition. Peak heating rates occurred at reattachment.

Schaeffer and Ferguson

Another experimental study of heat transfer in the vicinity of conical flares was made by Schaeffer and Ferguson (Ref. 35). Their model differed slightly from that of Becker and Korycinski in having a conical rather than an ogive nose. Tests were conducted in a 1-foot wind tunnel at a free-stream Mach number of 4.98. Reynolds numbers per foot ranged from 1.6×10^6 to 5.4×10^6 resulting in laminar, turbulent, and transitional boundary layers. Flare half-angles of 10, 17, 24, and 56 degrees were investigated. The flare-cylinder juncture was 11.33 inches from the nose of the model, or approximately 6.3 body diameters.

The model, instrumented to measure pressure and heat-transfer distributions, was cooled to 120°R before being injected into the airstream. Heating rates were determined by the transient thin-skin method neglecting conduction and radiation losses. Accuracy of the heat-transfer data was estimated at ±20%. Heat-transfer results were presented in the form of free-stream Stanton number.

Separation occurred with the laminar and transitional boundary layers, but not with the turbulent boundary layer. The length of the separated region decreased with wall-cooling, decreasing flare angle, and increasing Reynolds number. Minimum heat transfer occurred slightly downstream of separation. Contrary to the results of most of the other studies (Ref. 30, 31, 34, and 36), heat transfer in the separated laminar regions was not below the attached value. Sharp increases in heat transfer occurred during transition and reattachment. Peak heat transfer in the pure laminar case occurred downstream of reattachment and was much greater than the theoretical attached value. Peak heating in the transitional case occurred in the reattachment region. Peak turbulent heat transfer was predicted adequately by assuming the boundary layer started at the flare-cylinder junction.

Gulbran, and Others

Three-dimensional shock wave-laminar boundary layer interactions were the subject of a study made by Gulbran and others (Ref. 36). The shock wave was generated by a fin mounted perpendicular to a sharp leading-edge flat plate. The test was performed in a 50-inch-diameter wind tunnel at a free-stream Mach number of 8 and free-stream Reynolds numbers per foot ranging from 0.67×10^6 to 3.0×10^6. Parameters varied, in addition to Reynolds number, were fin leading-edge sweep and bluntness, fin and plate angle of attack, and chordwise position of the fin.

The flat plate, instrumented to measure pressure and heat-transfer distributions, was cooled to 0°F before being injected into the airstream. The test section of the plate extended approximately 7 inches from the leading edge. Heating rates were determined by the transient thin-skin method, with corrections made for conduction losses when necessary. Data were presented in the form of pressures and heat-transfer coefficients nondimensionalized by theoretical flat-plate values.

Results indicated that the peak pressure and heating rates increased with increasing fin deflection, decreasing sweep angle, and increasing leading-edge diameter. Peak heating rates were also increased by moving the fin forward. Angle of attack of the flat plate had little effect on the peak heating rates. Boundary-layer separation occurred in nearly all test runs. Heat-transfer coefficient distributions exhibited the familiar trend for laminar interactions of falling below the attached value in the separated region and in reaching a peak slightly downstream of reattachment.

Miller, and Others

As an earlier part of the study of Gulbran (Ref. 36), Miller and others (Ref. 37) investigated hypersonic fin-shock interactions on a laminar boundary layer. The unswept, sharp leading-edge fin was mounted on a sharp leading-edge flat plate instrumented to measure pressure and heat-transfer distributions. The fin angle was varied from -10 degrees (expansion) to +15 degrees (compression). Tests were conducted in a 44-inch wind tunnel at a free-stream Mach number of 16 and Reynolds numbers per foot ranging from 0.04×10^6 to 1.0×10^6. At this high Mach number, interactions between the leading-edge shock and the boundary layer will probably exist; however, the results of the study were included for interest in the correlations presented.

Heating rates were measured with thermistor heat-flux gages. Heat-transfer data were presented in the form of free-stream Stanton number. Measured pressures were nondimensionalized by the free-stream static pressure.

Heat-transfer results indicated that boundary-layer transition occurred at compression angles greater than 10 degrees. Pressure and heat-transfer distributions did not indicate the presence of separation.

Experimental investigations of heat transfer on conical flares and deflected flaps also were made by utilizing free-flight testing (Ref. 38 and 39). These results were not used in the present correlations because of the relative inaccuracy of measurements made during free flight as compared with wind-tunnel testing.

EXISTING EMPIRICAL RELATIONS FOR PEAK HEAT TRANSFER

Several of the experimental investigators used their test results to develop empirical expressions for determining the peak heat transfer in shock interaction regions. Most of these expressions were developed with a limited amount of data for a specific configuration. Relations that were presented in some of the studies discussed in the previous section are described below.

Levin and Fabish

An expression for peak Stanton number in the interaction region of an impinging planar shock wave on a turbulent flat-plate boundary layer was developed by Levin and Fabish, from their experimental data (Ref. 27). They suggested the following relation between the peak Stanton number and the peak pressure ratio:

$$\left(\frac{St_e}{St_1}\right)_{PK} = K_1 \quad \text{for} \quad \left(\frac{P_3}{P_1}\right) < \left(\frac{P_3}{P_1}\right)_B$$

$$\left(\frac{St_e}{St_1}\right)_{PK} = K_1 + K_2\left[\left(\frac{P_3}{P_1}\right) - \left(\frac{P_3}{P_1}\right)_B\right] \quad \text{for} \quad \left(\frac{P_3}{P_1}\right) > \left(\frac{P_3}{P_1}\right)_B$$

The constant K_1 has a value from approximately 1.4 to 1.8; K_2 is approximately 1.45; and the reference value $(P_3/P_1)_B$ is a function of the mass flow ratio $(\rho V)_3/(\rho V)_1$.

Sayano

A relation between peak heat transfer and peak pressure was presented in Sayano's study (Ref. 28). The expression for turbulent interactions arising from planar shock impingement on flat plates or cylinders is

$$\frac{h_{PK}}{h_{FP}} = \left(\frac{P_{PK}}{P_{FP}}\right)^{0.8}$$

The peak pressure ratio was also related to the incident shock strength; the resulting expressions for peak heat transfer are

$$\text{Flat Plate Impingement:} \quad \frac{h_{PK}}{h_{FP}} = \left(\frac{P_2}{P_1}\right)^{1.4}$$

$$\text{Cylinder Impingement:} \quad \frac{h_{PK}}{h_{FP}} = \left(\frac{P_2}{P_1}\right)^{1.22}$$

Popinski

Popinski performed peak heat-transfer correlations using both his laminar data and the results of other investigations. The following expression was obtained for the case of laminar interactions in two-dimensional compression corners:

$$\frac{h_{PK}}{h_{FP}} = \frac{5.0 \times 10^6 \left(P_2/P_0\right)^{0.88}}{\left(Re_{\infty_{x_0}}\right)^{1/2} M_\infty^{3.7}}$$

For separated turbulent interactions caused by shock impingement, he suggested the following relation between peak heat transfer and plateau pressure

$$\frac{h_{PK}}{h_{FP}} = 1.18 \left(\frac{P_3 - P_{PL}}{P_0}\right)^{0.185} M_\infty$$

For the case of turbulent interactions without separation, peak heat transfer was related to pressure ratio and Reynolds number as follows:

$$\frac{h_{PK}}{h_{FP}} = \frac{29.5 \left(P_3/P_1\right)^{0.709}}{\left(Re_{\infty_{x_0}}\right)^{1/5}}$$

Both of the turbulent relations were obtained from the data of Levin and Fabish (Ref. 27) and Sayano (Ref. 28).

In addition to peak heat-transfer correlations, Popinski developed empirical expressions for several other interaction parameters such as plateau pressure, interaction length, and separation length.

Gulbran, and Others

The results of Gulbran and others (Ref. 36) for laminar fin-shock interactions indicated that the governing variable for the peak heat transfer was the rise from plateau pressure to peak pressure. They proposed the following empirical expression:

$$\frac{h_{PK}}{h_{FP}} = 2.9 \left(P_F - P_{PL}\right)^{0.3} \left(\frac{P_F}{P_{PL}}\right) \left(\frac{P_{PL}}{P_{PL_{REF}}}\right)^{0.15}$$

In this particular correlation, $P_{PL_{REF}}$ is for the case of a sharp leading-edge unswept fin at 7.5 degrees deflection. The plateau pressure, P_{PL}, is calculated by the method of Erdos and Pallone (Ref. 40), and the final pressure, P_F, is obtained from oblique shock theory.

Shumway

Results of several experimental studies were used by Shumway (Ref. 32) to obtain a relation for the peak heat transfer in shock wave boundary layer interaction regions. He suggested the following linear relation between peak heat-transfer coefficient and peak pressure in the interaction region:

$$\frac{h_d}{h_u} = \frac{P_d}{P_u}$$

This expression was obtained by using data from laminar and turbulent interactions generated by compression corners, impinging shock waves, and fin shocks. The subscripts d, downstream, and u, upstream, used by Shumway are equivalent to the subscripts PK, peak, and FP, flat plate, which are used in the studies mentioned previously.

A similar expression can be obtained by order-of-magnitude analysis, as shown by Giles and Thomas (Ref. 41). Because of certain assumptions made in the analysis, the authors recommend that this result be used only in a qualitative sense.

For cases in which shock interaction causes transition, Shumway suggests a relation based on the following laminar and turbulent expressions for Stanton number:

$$St_{LAM} = 0.332\ Pr^{-2/3}\ Re^{-0.5}$$

$$St_{TURB} = 0.0288\ Pr^{-2/3}\ Re^{-0.2}$$

The ratio of these expressions, taken across a shock wave, gives

$$\frac{h_d}{h_u} = 0.089\ \frac{(\rho V)_d^{0.8}}{(\rho V)_u^{0.5}}\ \frac{\mu_d^{0.2}}{\mu_u^{0.5}}$$

Section 4

PRESSURE AND HEAT TRANSFER DISTRIBUTIONS

Schematic representations indicating the nomenclature used to define the geometry of the impinging-shock, compression-corner, and fin-shock interactions are given in Fig. 10. Qualitative distributions of pressure and heat-transfer coefficient in interaction regions are shown in Fig. 11 and 12, respectively. The reference position, shown in these figures, represents the point of geometric shock impingement in the case of the impinging shock; the corner for wedge or conical flare interactions; and in the case of the fin shock, the location where the shock is incident on the surface.

When analyzing shock wave-boundary layer interactions, it is first necessary to know whether the interaction is laminar (transition downstream of interaction); turbulent (transition upstream of interaction); or transitional (transition within interaction region). Unfortunately, no completely reliable way is known for predicting whether or not the latter will occur.

It is also necessary to determine if the boundary layer is separated or attached. Some relations have been developed for predicting the occurrence of separation. Incipient separation is defined as the condition under which flow first begins to separate. Separation will occur, therefore, if the overall pressure rise associated with the interaction is greater than the pressure rise required for incipient separation. This pressure is sometimes termed the critical pressure.

Using the results of a study of shock impingement on laminar boundary layers, Hakkinen and others (Ref. 26) obtained the following relation between the pressure coefficient required for incipient separation, $C_{P_{INC}}$, and the pressure coefficient at the separation point, $C_{P_{SEP}}$:

$$C_{P_{INC}} = 2\, C_{P_{SEP}}$$

The following empirical expression for separation pressure in laminar interactions was developed by Popinski (Ref. 30) and is based on tests of several configurations:

$$C_{P_{SEP}} = 0.91 \left(M_1^2 - 1\right)^{-0.287} Re_{\infty_{x_0}}^{-1/4}$$

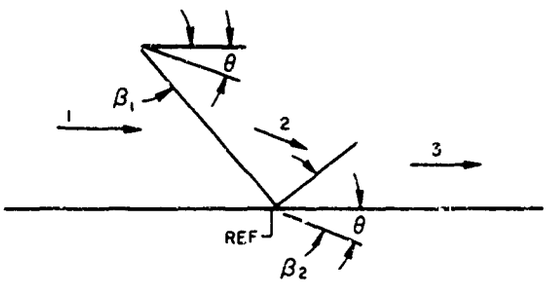

(a) Shock Impingement on Flat Plate or Cylinder.

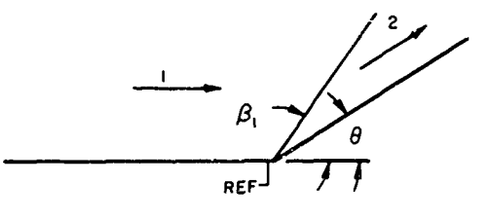

(b) Compression Corner With Attached Boundary Layer.

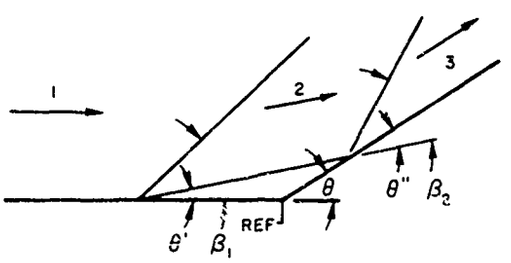

(c) Compression Corner With Separated Boundary Layer.

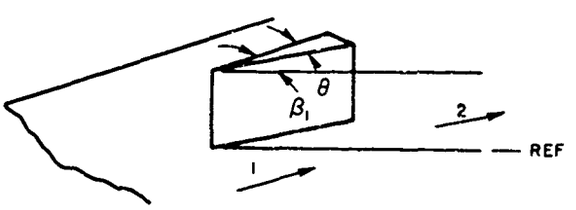

(d) Fin Shock.

FIG. 10. Representation of Nomenclature Used to Describe Interaction Parameters.

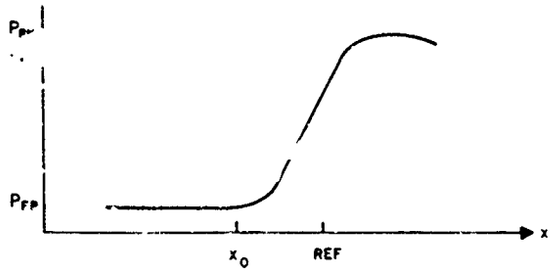

(a) Attached Boundary Layer.

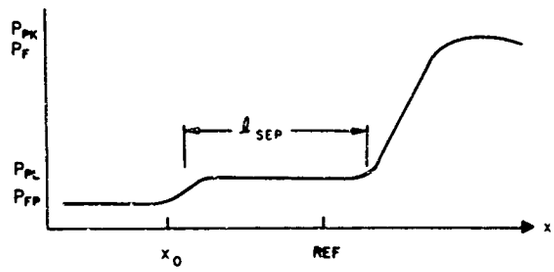

(b) Separated Laminar Boundary Layer.

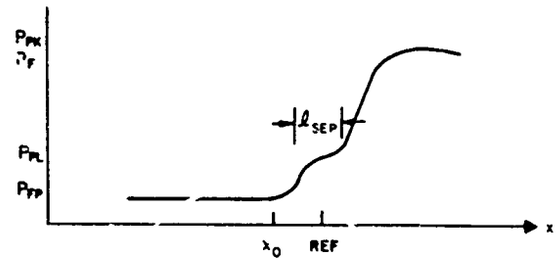

(c) Separated Turbulent Boundary Layer.

FIG. 11 Qualitative Pressure Distributions in Shock Wave-Boundary Layer Interaction-Regions.

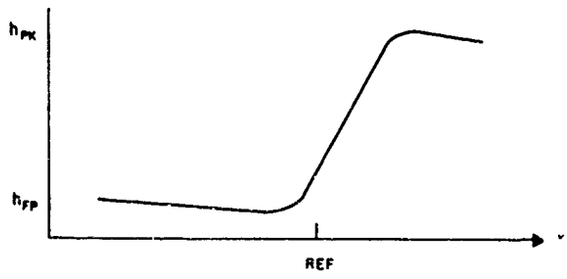

(a) Attached Boundary Layer.

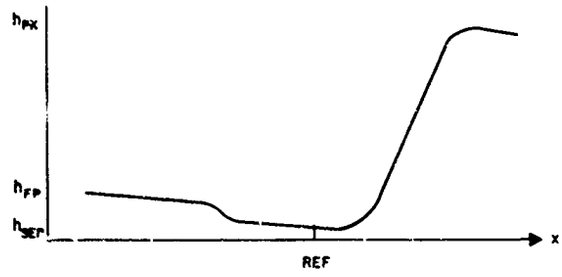

(b) Separated Laminar Boundary Layer.

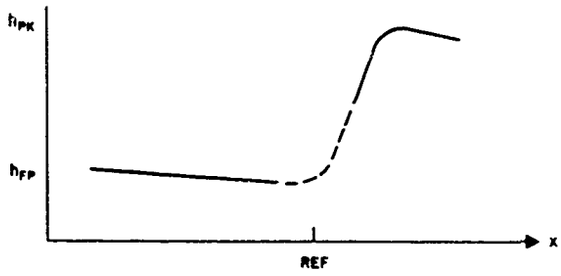

(c) Separated Turbulent Boundary Layer.

FIG. 12. Qualitative Heat-Transfer Coefficient Distributions in Shock Wave-Boundary Layer Interaction-Regions.

Combining the two equations gives

$$C_{P_{INC}} = 1.82 \left(M_1^2 - 1\right)^{-0.287} Re_{\infty_{x_0}}^{-1/4}$$

The Reynolds number in this equation is calculated at the beginning of the interaction region, x_0. However, if x_0 is large compared to the length of interaction region, the Reynolds number may be evaluated at x_{REF} without having an appreciable effect on $C_{P_{INC}}$. Although the relation between $C_{P_{INC}}$ and $C_{P_{SEP}}$ is based on data from impinging shock interactions, it should be valid for all configurations because of the free-interaction concept, which states that the upstream portion of the interaction is independent of the means of generating the pressure gradient (Ref. 25).

The following expression for incipient separation in turbulent boundary layers was developed by Popinski who used compression corner data:

$$C_{P_{INC}} = 1.36 \left(M_1^2 - 1\right)^{0.193} Re_{\infty_{x_0}}^{-1/10}$$

As in the case of laminar separation, this expression should be applicable to other configurations because of the concept of free interaction.

PRESSURE DISTRIBUTION

Figure 11 indicates the importance of the state of the boundary layer on the pressure distribution through an interaction region. If the boundary layer remains attached, the pressure rises smoothly from the undisturbed value to the peak value. The pressure rise in a laminar interaction will take place over a considerably longer distance than it will in the case of a turbulent interaction. This is because of the lower kinetic energy of the laminar boundary layer allowing the pressure disturbance to propagate farther upstream. If the boundary layer separates, the pressure increases at the separation and reattachment points, and a pressure plateau forms in the separated region. In separated turbulent flow, the plateau will often appear as an inflection point because the separated region is of relatively short length. In addition to the separation and reattachment pressure rises, pressure

rises have been observed in transition regions of separated flows. A detailed discussion of the effects of the state of the boundary layer on the pressure distribution may be found in the work of Chapman, Kuehn, and Larson (Ref. 25). Plateau pressure, peak pressure, and the inviscid final pressure are used in the present heat-transfer correlations.

Plateau Pressure

A region of constant pressure, designated the plateau pressure, has been observed to exist in separated regions. Plateau pressure is governed by the concept of free interaction and is a function only of the upstream Mach number and Reynolds number. Analysis (Ref. 25) has shown that

$$C_{P_{PL}} \sim \left[\frac{C_f}{\left(M_1^2 - 1 \right)^{1/2}} \right]^{1/2}$$

With the use of the following equations for laminar and turbulent local skin friction (Ref. 42),

$$C_{f_{LAM}} = 0.664 \, Re_x^{-1/2}$$

$$C_{f_{TURB}} = 0.0576 \, Re_x^{-1/5}$$

expressions for laminar and turbulent plateau pressures are

$$C_{P_{PL_{LAM}}} = K_L \left(Re_x \right)^{-1/4} \left(M_1^2 - 1 \right)^{-1/4}$$

$$C_{P_{PL_{TURB}}} = K_T \left(Re_x \right)^{-1/10} \left(M_1^2 - 1 \right)^{-1/4}$$

Several values of the constants K_L and K_T were proposed from the results of various studies (Ref. 26, 40, and 43). For the present correlations, the values $K_L = 1.6$ and $K_T = 1.7$ are used, as given in the study of Wuerer and Clayton (Ref. 43). Plateau pressures calculated by using the preceding equations, and experimental plateau pressures obtained from the studies used in the present correlations are compared in Fig. 13. The agreement is satisfactory, with the exception of two data points (Ref. 35). Some of the scatter can be attributed to the difficulty of identifying the plateau pressure in several of the experimental pressure distributions.

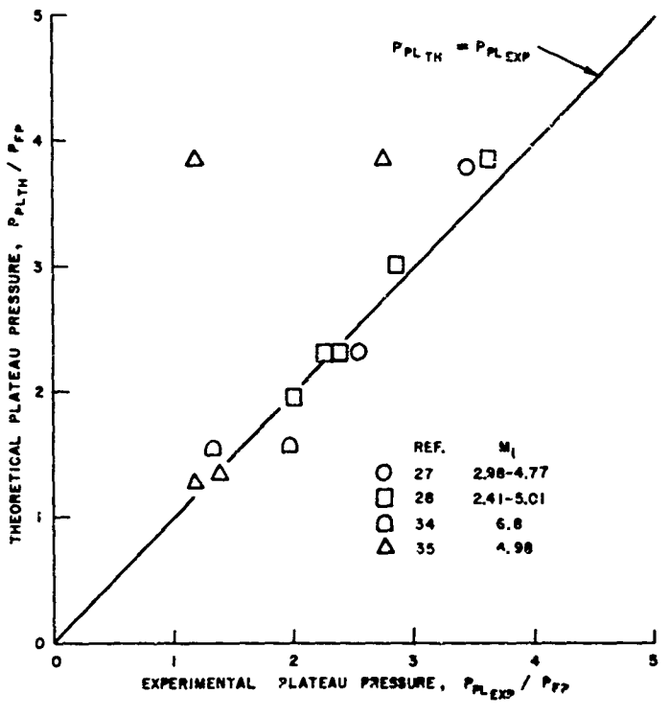

FIG. 13. Comparison of Theoretical and Experimental Plateau Pressures.

In the case of certain configurations, the plateau pressure may be used to estimate the length of the separated region. The flow-deflection angle in the separated region, θ', can be obtained from the plateau pressure and upstream Mach number by using inviscid shock relations. If either the separation or the reattachment points are known on a compression corner, the separation length may be determined geometrically by using the flow-deflection angle.

Peak and Final Pressures

After passing through the shock wave, the pressure distribution reaches a peak value which may or may not exceed the theoretical inviscid pressure-rise to the final pressure behind the interaction. Analytical means for predicting the peak pressure associated with shock wave-boundary layer interactions have been developed (Ref. 44 and 45). In most cases, however, the theoretical final pressure is a good approximation of the peak pressure. In Fig. 14, the corresponding final pressures are plotted against the experimental peak pressures obtained from the studies used in the correlations presented. Final pressures are calculated by using the applicable inviscid shock theories as described below. A more detailed description, including the equations involved, is given in the Appendix.

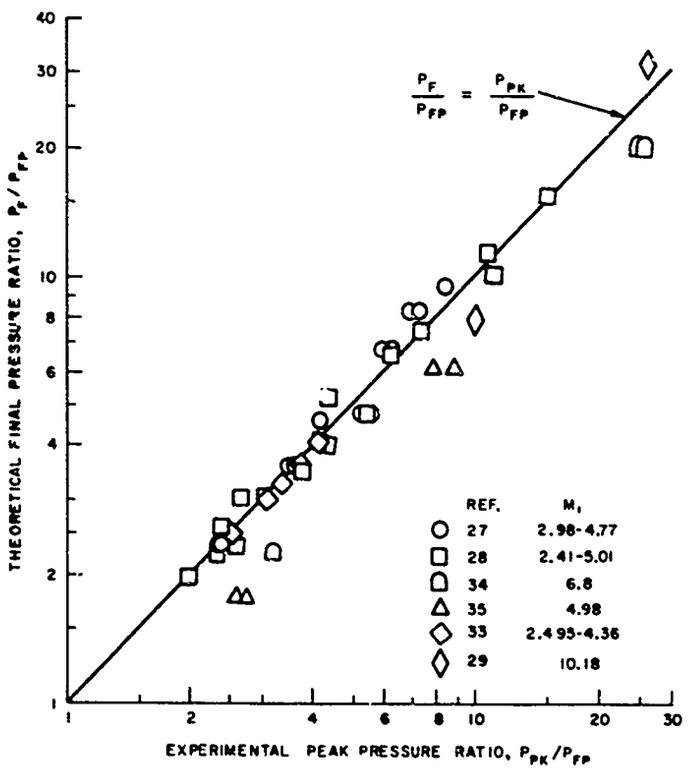

FIG. 14. Comparison of Theoretical Final Pressure With Experimental Peak Pressure.

Shock Impingement on Flat Plate or Cylinder. For the case of shock impingement and reflection (Fig. 10(a)), the pressure rise across the incident shock is calculated from the upstream Mach number and the shock-generator deflection angle with the use of the oblique shock relations (Ref. 46). The pressure rise across the reflected shock to the final pressure is calculated from the Mach number behind the incident shock with a turning angle equal to the shock-generator angle so that the flow is turned back parallel to the surface. The reflected shock is assumed to be oblique for the flat-plate interaction and conical for the cylinder interaction.

Wedge Compression-Corner. The pressure-rise across an attached-wedge interaction (Fig. 10(b)) is calculated from the upstream Mach number and the wedge angle. If the flow separates, the pressure rise is assumed to take place through a double compression. The initial pressure rise is assumed to be the plateau pressure calculated from the plateau pressure equations given on page 28. The flow-deflection angle is calculated from the plateau pressure and the upstream Mach number. The rise from plateau pressure to final pressure is then calculated by using the Mach number behind the separation shock and by assuming that the flow turns parallel to the wedge surface. Since the plateau pressure is based on skin friction, this is not truly an inviscid pressure rise. The double-compression pressure rise may be approximated by assuming that the separation angle is half the size of the wedge angle. Figure 15 shows how the final pressure varies with separation angle for a 20-degree wedge at Mach 4. Since the separation angle is usually small compared to the overall turning angle, this approximation will yield conservative results.

Conical Flare Compression-Corner. The pressure rise across attached or separated conical-flare interactions was calculated in the same manner as that of the wedge interactions, with the exception that empirical conical shock relations (Ref. 47) were used rather than the oblique shock relations.

Fin Shock. The pressure rise across a fin-generated shock wave (Fig. 10(d)) was calculated from the upstream Mach number and the fin-deflection angle by using the oblique shock relations.

In some cases, detached shock waves were predicted, and as a result solutions for final pressures were not obtained.

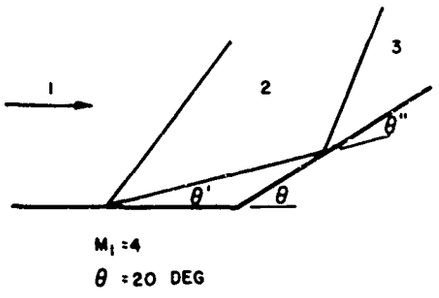

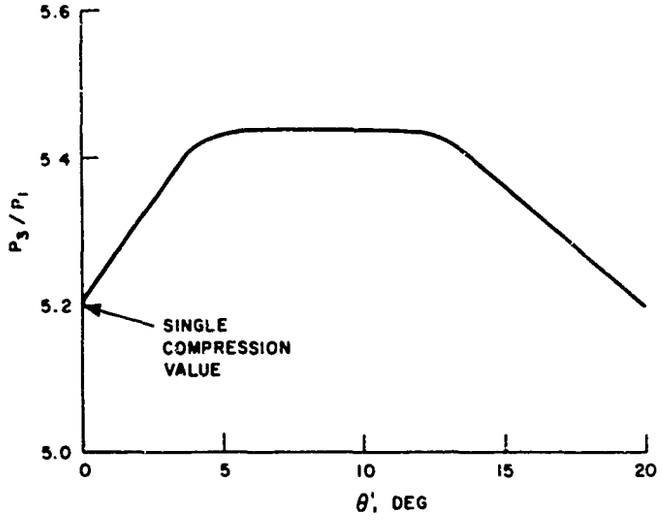

FIG. 15. Variation of Inviscid Pressure Ratio With Separation Angle.

HEAT-TRANSFER COEFFICIENT DISTRIBUTION

As would be expected, the heat-transfer coefficient distribution, shown qualitatively in Fig. 12, is strongly dependent on the state of the boundary layer in the interaction region as is the pressure distribution. Ii the boundary layer remains attached through the interaction, the heat-transfer coefficient distribution follows the same trend as that of the pressure distribution, increasing relatively smoothly from the beginning of the interaction to the peak value. If the boundary layer separates, or if transition occurs in the interaction region, the heat-transfer coefficient distribution becomes considerably more involved. The areas of interest in the heat-transfer coefficient distributions are heat transfer in the separated region and peak heat transfer.

Heat-Transfer Coefficients in Separated Regions

Analysis of separated flow is complicated because it is difficult to obtain repeatable experimental results in consecutive runs, let alone to compare results from different facilities (Ref. 41). Some of the trends which have been noticed are discussed below.

Laminar Separation. There is a definite decrease in heat-transfer coefficient in separated laminar regions. Chapman (Ref. 48) performed a theoretical analysis which indicated that the average laminar separated heating rate was 56% of the attached laminar value. This is in agreement with several experimental studies (Ref. 30, 34, 49, 50, and 51) that show the separated value to be approximately half the attached value.

Turbulent Separation. No reliable means for predicting heat transfer in separated turbulent flows is known. Chapman (Ref. 48) conducted a limited analysis showing heating rates above the attached values, with the rate of heating-increase decreasing as the Mach numbers increased. Most experimental studies show the separated turbulent heat-transfer to be above the attached value (Ref. 28, 51, and 52); however, heating rates below the attached value have been measured (Ref. 49). Semi-empirical relationships for the calculation of Stanton number in regions of turbulent separated flows were developed by Spalding (Ref. 53) that satisfactorily correlate with experimental results.

Peak Heat-Transfer Coefficient

Peak heat transfer in shock wave-boundary layer interaction regions is usually of the utmost interest. Heat-transfer coefficient increases of 10 to the undisturbed value (the value which would exist with no interaction) are common; in cases where the interaction causes transition, increases of over 30 times the undisturbed value have been measured. The seriousness of a high local heat-transfer coefficient is related to the thermal properties of the material involved. If the surface material has a high thermal conductivity, heat conduction away from the region of high heating rate will provide relief from thermal gradients. If the thermal conductivity is low, however, heat conduction will be much less, and a hot spot will develop.

Peak measured heating rates have usually been observed in the vicinity of reattachment where the boundary layer is thinnest, or if separation does not occur, immediately downstream of shock interaction. Increased mixing rates in the interaction region contribute to the increase in heat transfer. Some success has been achieved in predicting peak heat transfer by assuming that a new boundary layer starts at shock impingement or at a compression corner for attached flows, and at reattachment for separated flows. As mentioned previously, several correlations of peak heat transfer have been made for specific configurations. In Section 5, experimental peak heat-transfer coefficients for several configurations are correlated with various parameters.

Little work has been done on the decay of heat-transfer coefficient distribution downstream of shock wave-boundary layer interactions.

INTERACTION GEOMETRY

Interaction Lengths

Several correlations of the interaction lengths that are required to define the pressure and heat-transfer distributions were developed by Popinski (Ref. 30). Expressions are presented for interaction lengths upstream and downstream of both laminar and turbulent boundary-layers. The correlations are divided into impinging-shock data and compression-corner data, and in most cases they represent extremely limited Mach number ranges. The correlating parameters are Mach number, Reynolds number, and plateau pressure. Further data of this nature are required before expressions for general application can be obtained.

Separation Length

Estimates of length of the separated region for laminar (Ref. 41) and for turbulent (Ref. 30) boundary layers have been made by combining impinging-shock and compression-corner data. Although the separation length is defined as the distance from separation to reattachment, the turbulent correlation is for the distance from separation to the reference line. Turbulent separation is usually small enough so that the pressure and heat-transfer coefficient distributions can be approximated by linear increases over the interaction region. The expressions for laminar and for turbulent separation lengths are shown below.

$$\text{Laminar:}\quad \frac{\ell_{SEP}}{\delta_0} = \frac{35}{M_1^3}\left[\left(\frac{P_F - P_{PL}}{P_{FP}}\right) Re_{\infty_{x_0}}^{1/4}\right]^{0.98}$$

$$\text{Turbulent:}\quad \frac{\ell_{SEP}}{\delta_0} = 1.4 \times 10^5\, Re_{\infty_{x_0}}^{1/5}\left[\frac{\left(\frac{P_{PL}}{P_F} - 1\right)^{1.044}}{M_1}\right]^{16}$$

RECOVERY FACTOR

Another important aerodynamic-heating parameter which is affected by shock wave-boundary layer interaction is the recovery factor, defined as

$$r = \frac{T_{AW} - T_\infty}{T_T - T_\infty}$$

The adiabatic wall or recovery temperature is obtained from the free-stream temperature and Mach number by the relation

$$T_{AW} = T_\infty \left[1 + \left(r \frac{\gamma - 1}{2} M_\infty^2\right)\right]$$

The recovery factor is thus related to the aerodynamic-heating rate, as shown by the expression

$$q = h \left(T_{AW} - T_W\right)$$

Experimental studies have shown that the recovery factor in interaction regions is higher than the normal value, which is approximately 0.85 for laminar flow and 0.89 for turbulent flow. Means for predicting this increase do not exist. Since most of the studies determined the adiabatic wall temperature experimentally, effects of the variable recovery factor were automatically included in the data analysis. Some of the studies, however, assumed the appropriate recovery factor and calculated the adiabatic wall temperature. As a result, a portion of the apparent increase in heat-transfer coefficient was actually an increase in recovery factor. The errors caused by this approach more than likely were small compared to the overall experimental accuracy.

Section 5

PEAK HEAT-TRANSFER CORRELATIONS

Examination of existing experimental data led to the conclusion that the only thermal quantity in the interaction region for which meaningful correlations can be made, at the present time, is peak heat transfer. From an aerodynamic heating standpoint, this is probably the most important quantity in the interaction region. However, because of the extreme variations in heating rate that occur through the interaction, a complete analysis of a specific problem would require some knowledge of the heating rate distribution.

For this study, correlations of experimental peak heat-transfer coefficients were made with the following parameters:

1. Peak pressure measured in the interaction region
2. Theoretical final pressure
3. Theoretical plateau pressure
4. Reynolds number based on distance
5. Reynolds number based on boundary-layer thickness
6. Mach number

Data were utilized from tests performed on the following configurations:

1. Planar shock impingement on flat plate (Ref. 27, 28, and 29)
2. Planar shock impingement on cylinder (Ref. 28)
3. Compression corner, wedge (Ref. 30, 31, and 33)
4. Compression corner, conical flare (Ref. 34 and 35)
5. Fin mounted on flat plate (Ref. 36 and 37)

These data represent free-stream Mach numbers, ranging from 2.4 to 16 and Reynolds numbers based on distance from 7.9×10^5 to 8.09×10^6.

Pressures and heat-transfer coefficients are referenced to flat-plate values, which were obtained either experimentally or analytically, depending on how the original data were presented. The flat-plate values represent the conditions that would exist at the reference line (Fig. 10) in undisturbed flow. When practical, empirical expressions were obtained by fitting a straight line through the data points using the method of least squares. Parameters used in the correlations are summarized in Table 2. Results of the correlations follow.

PEAK PRESSURE

The first peak heat-transfer correlations attempted in this study were with the experimental peak pressures. Results of these correlations indicated that the relation between peak heat-transfer coefficient and peak pressure is independent of configuration, at least for the five configurations considered. The results also indicated that the correlations can be separately categorized as to whether the boundary layer is completely laminar, completely turbulent, or undergoes transition in the interaction region. Plots of peak heat-transfer coefficient versus peak pressure are shown for the laminar, turbulent, and transitional interactions in Fig. 16, 17, and 18, respectively. Considerable scatter exists in the laminar data, but the turbulent data correlates fairly well. Only a limited amount of transitional data are available for correlation purposes.

Empirical expression describing the correlations are

$$\text{Laminar:}\quad \frac{h_{PK}}{h_{FP}} = \left(\frac{P_{PK}}{P_{FP}}\right)^{1.29}$$

$$\text{Turbulent:}\quad \frac{h_{PK}}{h_{FP}} = \left(\frac{P_{PK}}{P_{FP}}\right)^{0.85}$$

$$\text{Transition:}\quad \frac{h_{PK}}{h_{FP}} = 6.4\left(\frac{P_{PK}}{P_{FP}}\right)^{0.63} \qquad \begin{pmatrix}\text{based on}\\ \text{limited data}\end{pmatrix}$$

TABLE 2. Summary of Test Results and Correlation Parameters

Ref.	Configuration	M_∞	θ, deg	M_1	Experimental $\frac{h_{PK}}{h_{FP}}$	Experimental $\frac{P_{PK}}{P_{FP}}$	Calculated $\frac{P_F}{P_{FP}}$	Calculated $\frac{P_{PL}}{P_{FP}}$	$Re_{x_{REF}} \times 10^{-6}$	$Re_\delta \times 10^{-4}$	Boundary layer
27	Flat plate	2.95	6	2.98	2.78	2.39	2.34	(a)	7.79	11.9	Turbulent
		2.95	6	2.98	2.44	2.35	2.34	(a)	7.79	....	Turbulent
		2.95	9.5	2.98	3.19	3.46	3.59	(a)	8.03	11.6	Turbulent
		2.95	9.5	2.98	3.16	3.56	3.59	(a)	8.03	....	Turbulent
		2.95	12	2.98	4.11	5.50	4.75	2.31	8.09	11.3	Turbulent
		2.95	12	2.98	3.79	5.25	4.75	2.31	8.09	....	Turbulent
		2.95	12	2.98	3.60	5.25	4.75	2.31	8.09	....	Turbulent
		5.02	7.4	4.77	4.70	4.15	4.60	(a)	4.31	....	Turbulent
		5.02	9.7	4.77	5.63	5.86	6.75	(a)	4.24	....	Turbulent
		5.02	9.7	4.77	5.35	6.16	6.75	(a)	4.24	....	Turbulent
		5.02	11	4.77	6.05	7.22	8.24	(a)	4.24	....	Turbulent
		5.02	11	4.77	6.06	7.25	8.24	(a)	4.24	....	Turbulent
		5.02	11	4.77	5.67	6.81	8.24	(a)	4.31	....	Turbulent
		5.02	12	4.77	7.39	8.41	9.52	3.79	4.24	....	Turbulent
		5.02	12	4.77	7.24	8.47	9.52	3.79	4.24	....	Turbulent
28	Flat plate	2.41	8	2.41	2.0	2.4	2.55	(a)	7.9	12.4	Turbulent
		2.41	15	2.41	3.4	4.3	5.16	1.95	7.9	12.4	Turbulent
		3.01	8	3.01	2.2	3.0	3.03	(a)	7.55	12.0	Turbulent
		3.01	15	3.01	4.6	6.2	6.58	2.31	7.55	12.0	Turbulent
		3.01	26	3.01	6.0	9.5	(b)	2.31	7.55	12.0	Turbulent
		3.99	8	3.99	3.2	4.0	4.06	(a)	7.05	11.3	Turbulent
		3.99	15	3.99	6.8	11.0	10.19	2.99	7.05	11.3	Turbulent
		5.01	15	5.01	9.2	15.0	15.53	3.86	5.35	9.0	Turbulent
28	Cylinder	2.41	8	2.41	1.6	2.1	2.0	(a)	7.77	12.2	Turbulent
		2.41	15	2.41	2.2	3.3	3.5	1.95	7.77	12.2	Turbulent
		3.01	8	3.01	2.2	2.6	2.3	(a)	7.17	11.5	Turbulent
		3.01	15	3.01	3.5	5.4	4.7	2.32	7.17	11.5	Turbulent
		3.99	8	3.99	2.6	2.7	3.0	(a)	6.97	11.2	Turbulent
		3.99	15	3.99	4.8	7.4	7.4	2.99	6.97	11.2	Turbulent
		5.01	8	5.01	3.3	4.3	4.0	(a)	3.88	7.0	Turbulent
		5.01	15	5.01	7.0	10.7	11.4	3.96	3.88	7.0	Turbulent
29	Flat plate	10.18	0	10.18	5	5	1	(a)	4.32	7.67	Turbulent
		10.18	5	10.18	7	10	7.95	(a)	5.04	8.66	Turbulent
		10.18	10	10.18	13	26	30.35	(a)	5.22	8.87	Turbulent
		9.98	10	9.98	20.5	26	30.35	(a)	0.79	0.45	Laminar
30	Wedge	8.13	9.5	7.8	9.4	....	5.17	1.67	2.30	0.76	Laminar
		8.12	15.0	7.8	19.8	....	10.52	1.68	2.11	0.73	Laminar
		8.07	13.9	7.8	17.6	....	9.18	1.73	1.59	0.63	Laminar
		8.02	9.4	7.8	17.1	....	5.02	1.79	1.11	0.53	Laminar
		8.12	18.5	7.4	30	....	15.23	1.69	2.07	0.72	Laminar
		9.7	10.0	9.1	10.8	....	7.32	1.94	1.71	0.65	Laminar
		9.7	13.7	9.7	22.1	....	12.54	1.94	1.68	0.65	Laminar
		9.68	10.0	9.2	16.3	....	7.30	1.97	1.45	0.62	Laminar
		9.7	10.0	8.5	23.6	....	20.93	1.95	1.63	0.64	Laminar

TABLE 2. (Continued)

Ref.	Configuration	M_∞	δ, deg	M_1	Experimental $\frac{h_{PK}}{h_{FP}}$	Experimental $\frac{P_{PK}}{P_{FP}}$	Calculated $\frac{P_F}{P_{FP}}$	Calculated $\frac{P_{PL}}{P_{FP}}$	$Re_{x_{REF}} \times 10^{-6}$	$Re_\delta \times 10^{-4}$	Boundary layer
31	Wedge	9.7	7.6	8	4.0	3.9	3.8	(a)	0.89	0.47	Laminar
		9.7	10.0	8	5.9	5.15	5.45	1.83	0.89	0.47	Laminar
33	Wedge	2.495	15	2.495	2.5	2.5	2.46	(a)	8.0	12.59	Turbulent
		3.23	15	3.23	3.0	3.05	3.00	(a)	7.98	12.55	Turbulent
		3.59	15	3.59	3.13	3.35	3.31	(a)	7.15	11.44	Turbulent
		3.97	15	3.97	2.9	3.7	3.67	(a)	5.99	9.92	Turbulent
		4.36	15	4.36	3.45	4.1	4.06	(a)	5.03	8.47	Turbulent
34	Conical flare	6.8	10	6.8	3.2	2.3	2.37	1.54	1.9	0.69	Laminar
		6.8	10	6.8	3.3	3.2	2.37	(a)	7.0	0.93	Turbulent
		6.8	30	6.8	13.3	25.6	19.49	(a)	6.3	0.86	Turbulent
		6.8	30	6.8	43.8	24.9	19.49	1.58	1.4		Transition
35	Conical flare	4.98	10	4.98	4.3	2.56	1.75	1.36	1.53	0.62	Laminar
		4.98	10	4.98	11.0	2.74	1.75	1.26	5.15		Transition
		4.98	24	4.98	29.0	8.64	6.0	1.26	5.15		Transition
		4.98	24	4.98	5.9	7.94	6.0	3.85	5.15	8.82	Turbulent
		4.98	56	4.98	9.2	9.5	(b)	3.85	5.15	8.82	Turbulent
36	Fin	8.0	7.5	...	3.0	2.9	...	...	...	...	Laminar
		8.0	7.5	...	5.4	2.8	...	...	...	...	Laminar
		8.0	7.5	...	6.9	2.8	...	...	...	...	Laminar
		8.0	15.0	...	6.2	6	...	...	...	...	Laminar
		8.0	15.0	...	10.0	6	...	...	...	...	Laminar
		8.0	15.0	...	12.1	6.05	...	...	...	...	Laminar
		8.0	.5	...	3.1	3.1	...	...	...	...	Laminar
		8.0	.5	...	5.6	3.07	..	...	...	...	Laminar
		8.0	7.5	...	7.0	2.8	...	...	...	...	Laminar
		8.0	15.0	...	6.0	4.8	...	...	...	...	Laminar
		8.0	15.0	...	9.5	6.7	...	...	...	...	Laminar
		8.0	15.0	...	14.0	6.6	...	...	...	...	Laminar
37	Fin	16.0	0	...	2.3	1.7	...	...	...	...	Laminar
		16.0	5	...	3.5	2.0	...	...	...	...	Laminar
		16.0	7.5	...	5.0	2.95	...	...	...	...	Laminar
		16.0	10	...	6.9	4.7	...	..	...	...	Laminar
		16.0	15	...	27	9.09	...	...	...	...	Transition

[a]No observed separation.
[b]Detached shock.

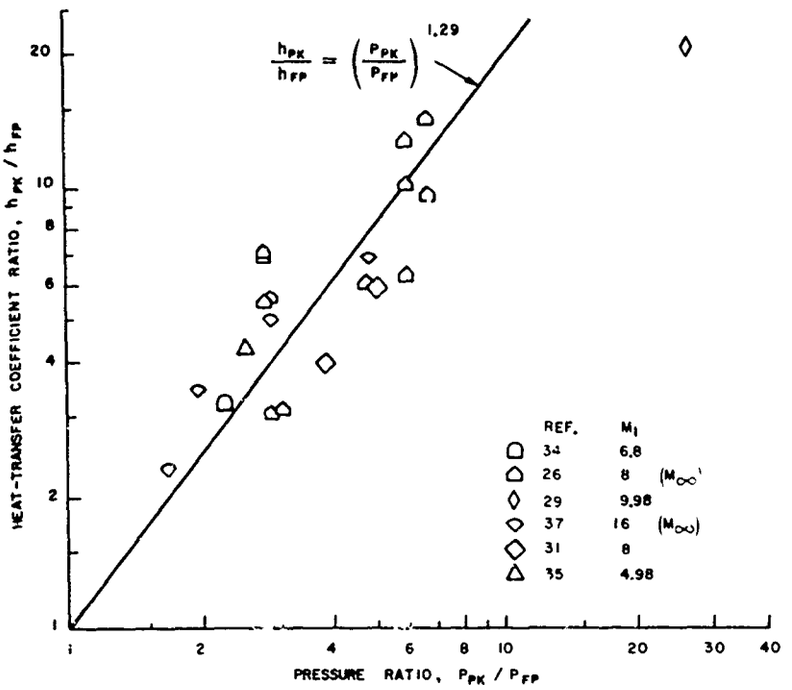

FIG. 16. Correlation of Peak Heat-Transfer Coefficient With Peak Pressure for Laminar Boundary Layer.

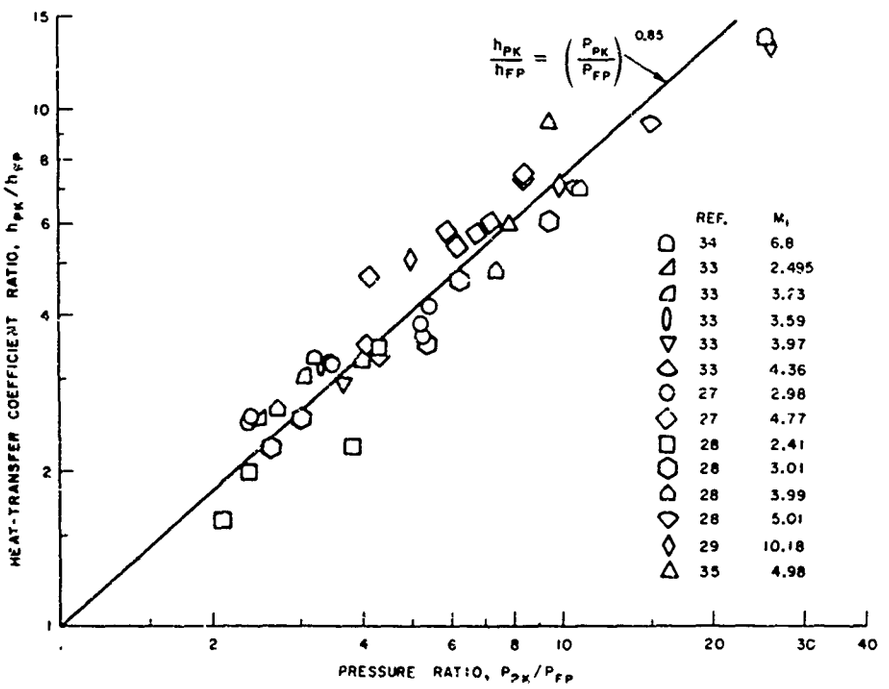

FIG. 17. Correlation of Peak Heat-Transfer Coefficient With Peak Pressure for Turbulent Boundary Layer.

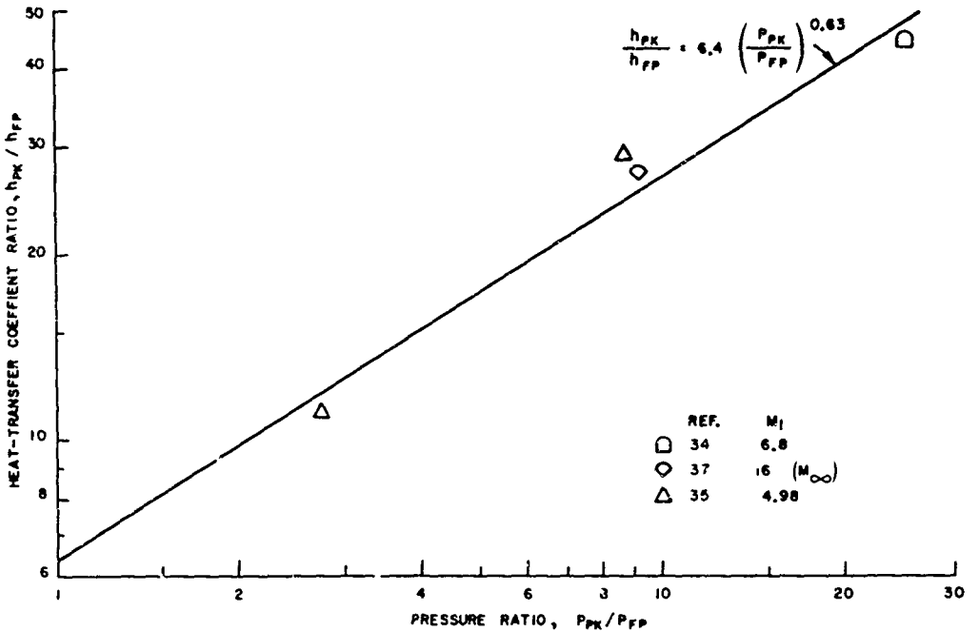

FIG. 18. Correlation of Peak Heat-Transfer Coefficient With Peak Pressure for Transition.

FINAL PRESSURE

The theoretical inviscid pressure-rise across a shock interaction, termed the final pressure, is a useful correlating parameter, for it describes the strength of the interaction and requires that only the upstream Mach number and the configuration be known. As shown in Fig. 14, the final pressure is also a good approximation of the peak pressure. Correlations of peak heat-transfer coefficient with final pressure for laminar, turbulent, and transitional boundary layers are shown in Fig. 19, 20, and 21, respectively. Final pressures were calculated as described in the Appendix. Fin-shock data (Ref. 36 and 37) are not included in the final pressure correlations because leading-edge effects on the flat plate caused the Mach number upstream of the interaction to differ from the Mach number generating the fin shock.

Because peak and final pressure are similar, these correlations show the same trends as those of the peak pressure correlations, with the turbulent correlations being considerably better than the laminar correlations.

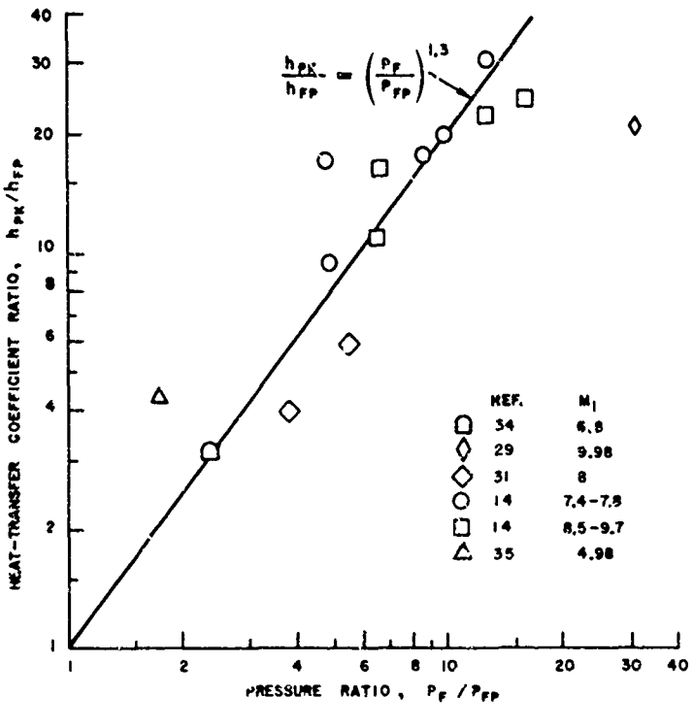

FIG. 19. Correlation of Peak Heat-Transfer Coefficient With Theoretical Final Pressure for Laminar Boundary Layer.

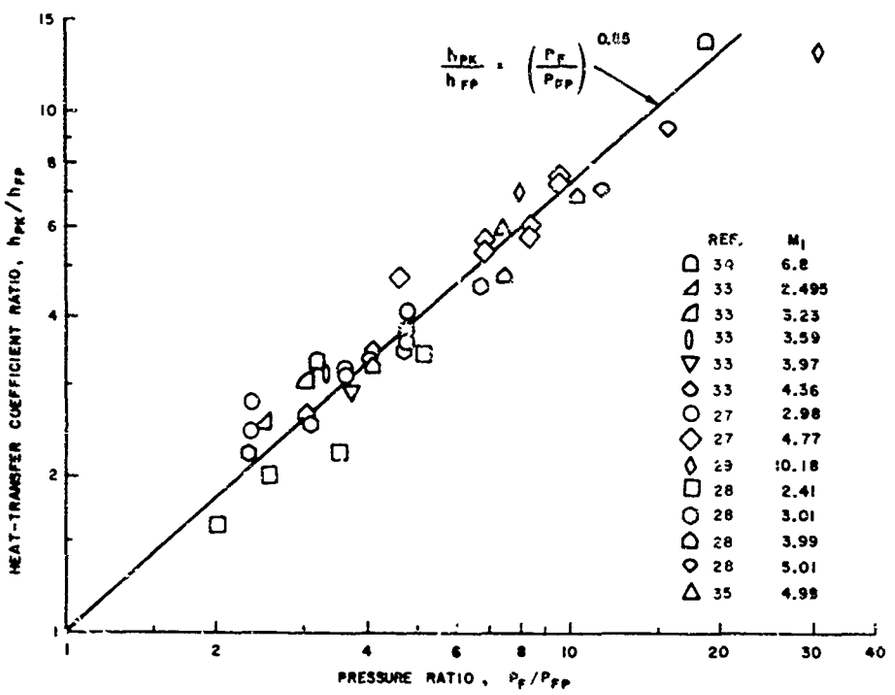

FIG. 20. Correlation of Peak Heat-Transfer Coefficient With Theoretical Final Pressure for Turbulent Boundary Layer.

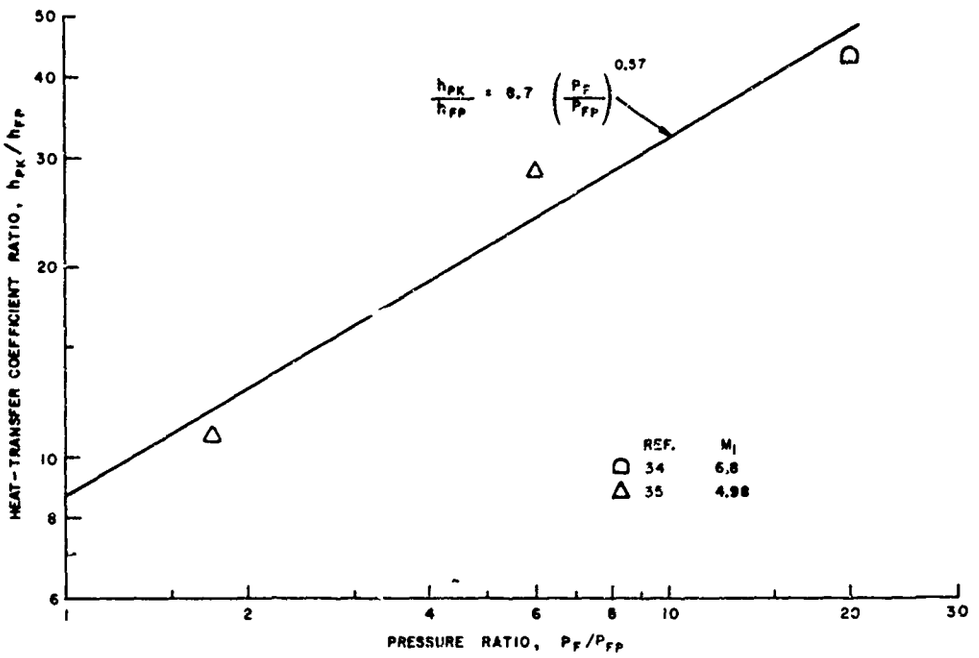

FIG. 21. Correlation of Peak Heat-Transfer Coefficient With Theoretical Final Pressure for Transition.

The following empirical expressions were obtained from the final pressure correlations:

$$\text{Laminar:} \quad \frac{h_{PK}}{h_{FP}} = \left(\frac{P_F}{P_{FP}}\right)^{1.3}$$

$$\text{Turbulent:} \quad \frac{h_{PK}}{h_{FP}} = \left(\frac{P_F}{P_{FP}}\right)^{0.85}$$

$$\text{Transition:} \quad \frac{h_{PK}}{h_{FP}} = 8.7 \left(\frac{P_F}{P_{FP}}\right)^{0.57} \qquad \left(\begin{matrix}\text{based on} \\ \text{limited data}\end{matrix}\right)$$

The turbulent expression is identical to that obtained in the peak pressure correlations.

PLATEAU PRESSURE

It is suggested in Ref. 36 that the peak heat-transfer in separated interactions is related to the rise from plateau pressure to final pressure. Correlations of peak heat-transfer coefficient with the quantities P_F/P_{PL} and $(P_F - P_{PL})/P_{FP}$ are made for the cases in which separation is known to exist. Plateau pressures are calculated from the equations given in Section 4. Laminar data correlated best with the quantity P_F/P_{PL}, whereas the turbulent data were best described by $(P_F - P_{PL})/P_{FP}$. Plots of these two correlations appear in Fig. 22 and 23, respectively. Plateau pressure correlations were not made with the transition data. Correlating peak heat-transfer with plateau pressure provided no improvement over the final pressure correlations. As in the previous cases, the laminar data exhibited considerably more scatter than did the turbulent data. The following expression relating peak heat-transfer to plateau pressure in turbulent interactions represents a least-squares fit of the data shown in Fig. 23. An expression was not derived for the laminar case because of the wide scatter in the data.

$$\frac{h_{PK}}{h_{FP}} = 1.9 \left(\frac{P_F - P_{PL}}{P_{FP}} \right)^{0.70}$$

REYNOLDS NUMBER AND MACH NUMBER

In an attempt to obtain better peak heat-transfer correlations, additional boundary-layer parameters were introduced. Parameters used were Reynolds number based on the reference distance (Fig. 10), Reynolds number based on the undisturbed boundary-layer thickness, and Mach number upstream of the interaction. The parameters were evaluated as described below.

Reynolds Number Based on Distance

Distance Reynolds numbers, $Re_{x_{REF}}$, were based on free-stream conditions and the distance from the leading edge of the model to the reference point, as defined in Fig. 10. As laminar and turbulent Stanton numbers are inversely proportional to the one-half and one-fifth powers, respectively, of Reynolds number, these values were used in the correlations.

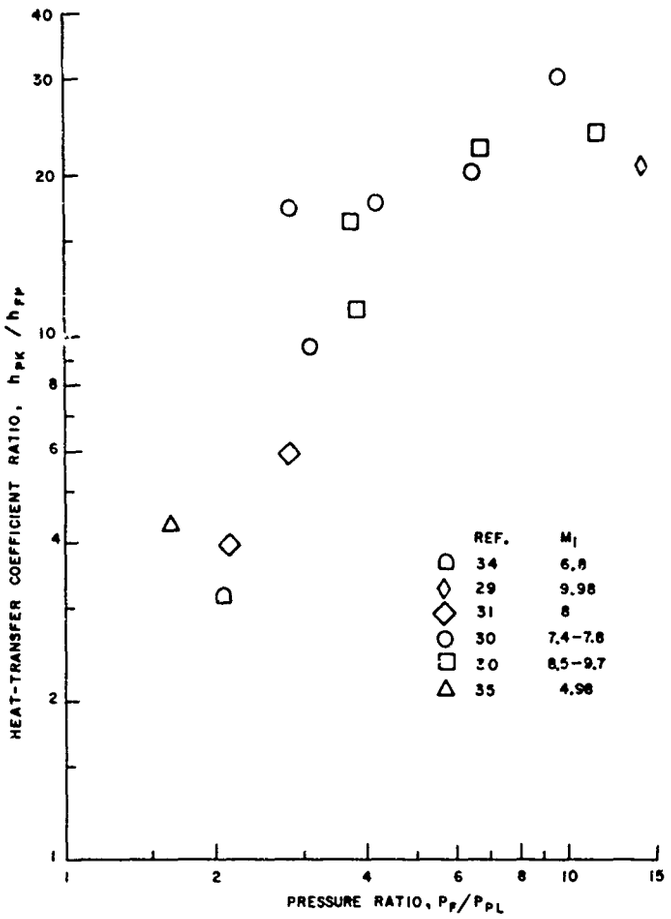

FIG. 22. Correlation of Peak Heat-Transfer Coefficient With Final and Plateau Pressure for Laminar Boundary Layer.

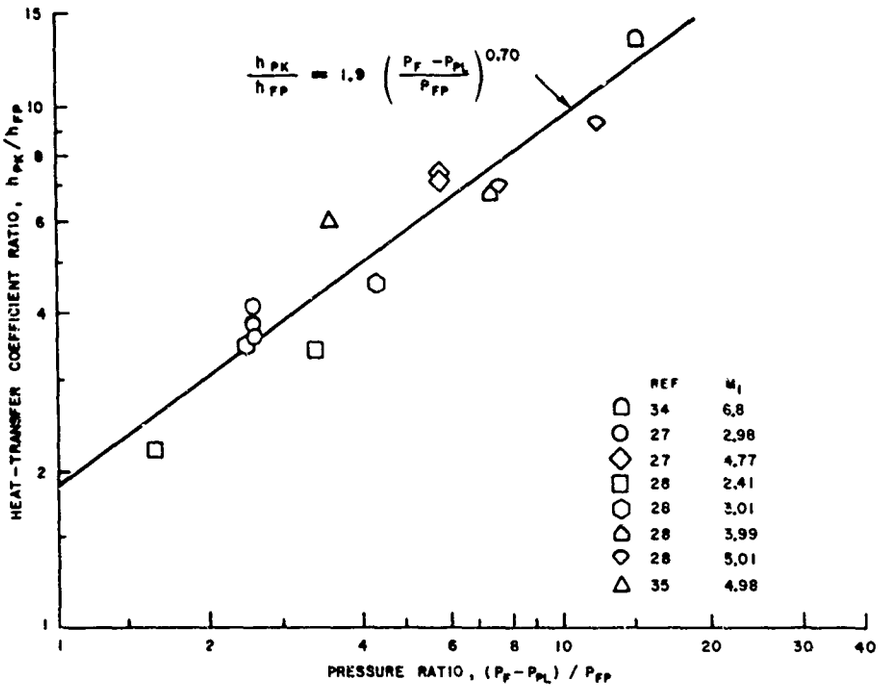

FIG. 23. Correlation of Peak Heat-Transfer Coefficient With Final and Plateau Pressures for Turbulent Boundary Layer.

Reynolds Number Based on Boundary-Layer Thickness

Because heat-transfer coefficient is dependent on boundary-layer thickness, it was felt that a Reynolds number based on boundary-layer thickness might provide a better correlation than would distance Reynolds number. Reynolds number was evaluated by using the hydrodynamic boundary-layer thickness at the reference point. The boundary-layer thickness was calculated from the following expressions (Ref. 42):

$$\text{Laminar:} \quad \delta = 5\, x_{REF} \left(Re_{x_{REF}}\right)^{-1/2}$$

$$\text{Turbulent:} \quad \delta = 0.376\, x_{REF} \left(Re_{x_{REF}}\right)^{-1/5}$$

The boundary-layer-thickness Reynolds number, Re_δ, was obtained as follows:

$$Re_\delta = \left(\frac{Re_{x_{REF}}}{x_{REF}} \right) \delta$$

$$Re_\delta = \frac{\left(\frac{\rho V x_{REF}}{\mu} \right)}{x_{REF}} K x_{REF} \left(\frac{\rho V x_{REF}}{\mu} \right)^{-a}$$

$$Re_\delta = K \left(\frac{\rho V x_{REF}}{\mu} \right)^{1-a}$$

$$Re_\delta = K \left(Re_{x_{REF}} \right)^{1-a}$$

Inserting the appropriate values for the constants, a and K, gives

$$\text{Laminar:} \quad Re_\delta = 5.0 \left(Re_{x_{REF}} \right)^{1/2}$$

$$\text{Turbulent:} \quad Re_\delta = 0.376 \left(Re_{x_{REF}} \right)^{4/5}$$

As in the case of the distance Reynolds number correlations, the one-half and one-fifth powers of boundary-layer-thickness Reynolds number were used in the laminar and turbulent correlations, respectively.

To attempt peak heat-transfer correlations with the change in boundary-layer thickness across the interaction region would have been desirable. However, this information is not included in the experimental data, and it can not be readily obtained analytically.

Upstream Mach Number

In most of the experimental data, the local Mach number upstream of the interaction, M_1, is either given or is essentially equal to the free-stream Mach number. In Ref. 30, Popinski calculated the local Mach number by assuming an isentropic compression through a weak leading-edge disturbance from the free-stream pressure to the static pressure on the plate surface. This procedure is described in detail in the Appendix.

The correlations attempted by using Reynolds number and Mach number and the results obtained for the laminar and the turbulent interactions follow.

Laminar Interactions

A peak laminar heat-transfer correlation, of the form suggested by Popinski (Ref. 30), is presented with the use of the parameters:

$$\frac{h_{PK}}{h_{FP}} Re_{x_{REF}}^{1/2} M_1^{3.7} \quad \text{versus} \quad \frac{P_F}{P_{FP}}$$

Popinski's correlating parameters differ slightly from these in that he used $Re_{\infty x_0}$ rather than $Re_{x_{REF}}$, and M_∞ rather than M_1. The difference in the two Reynolds numbers was small, and it was felt that use of the Mach number upstream of the interaction, rather than the free-stream Mach number, would make the correlation independent of leading-edge effects. This correlation, shown in Fig. 24, was unsuccessful.

Figure 25 shows the results of correlating peak heat-transfer with final pressure and Reynolds number based on the undisturbed boundary-layer thickness. This correlation

$$\frac{h_{PK}}{h_{FP}} Re_\delta^{1/2} \quad \text{versus} \quad \frac{P_F}{P_{FP}}$$

was also unsuccessful.

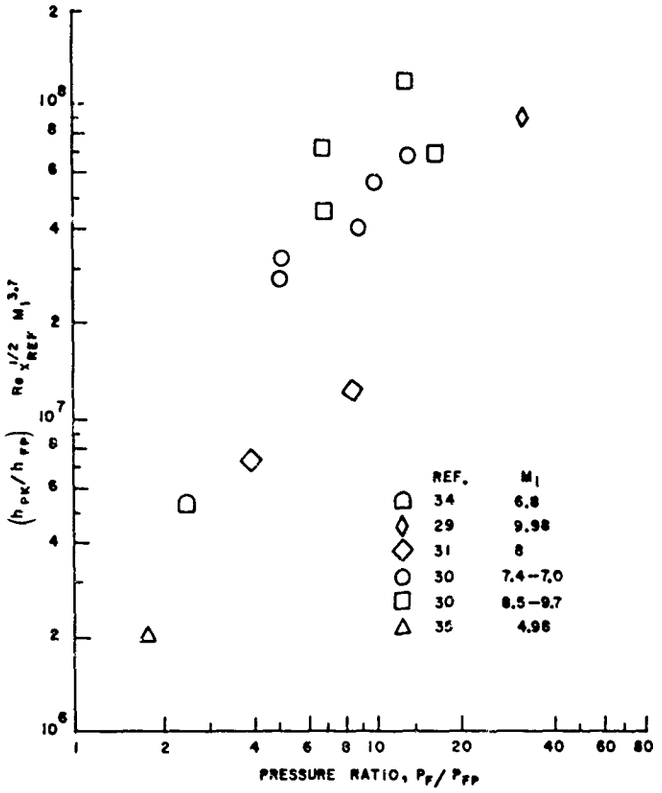

FIG. 24. Correlation of Peak Heat-Transfer Coefficient With Final Pressure, Reynolds Number, and Mach Number for Laminar Boundary Layer.

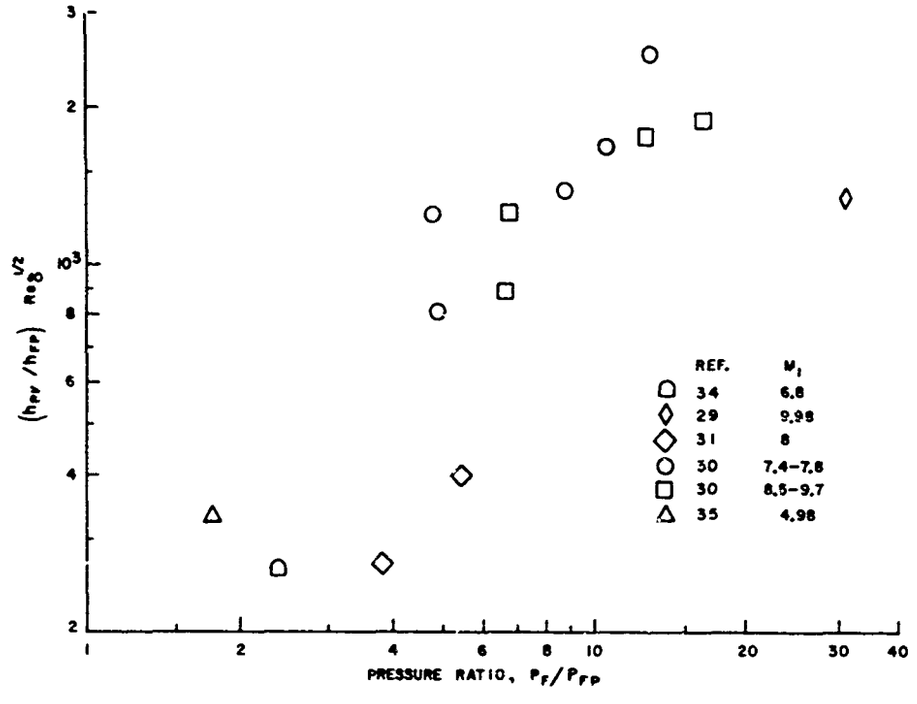

FIG. 25. Correlation of Peak Heat-Transfer Coefficient With Final Pressure and Reynolds Number Based on Boundary Layer Thickness for Laminar Boundary Layer.

The most promising of laminar correlations were obtained by introducing the quantity M_1^2. In Fig. 26, peak heat-transfer coefficient was correlated with M_1^2 and final pressure in the form

$$\frac{h_{PK}}{h_{FP}} M_1^2 \quad \text{versus} \quad \frac{P_F}{P_{FP}}$$

In Fig. 27, the Reynolds number based on boundary-layer thickness is included to give a correlation of the form

$$\frac{h_{PK}}{h_{FP}} Re_\delta^{1/2} M_1^2 \quad \text{versus} \quad \frac{P_F}{P_{FP}}$$

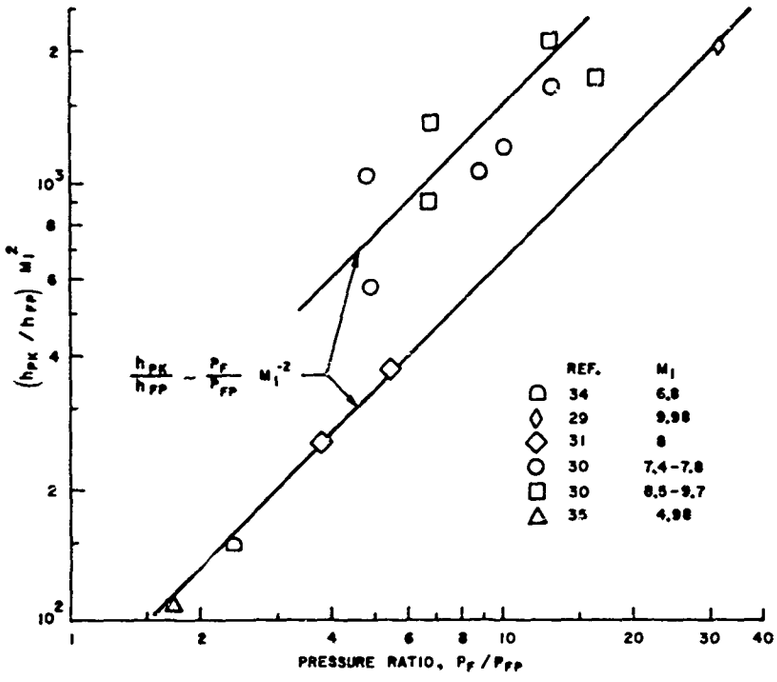

FIG. 26. Correlation of Peak Heat-Transfer Coefficient With Final Pressure and Mach Number for Laminar Boundary Layer.

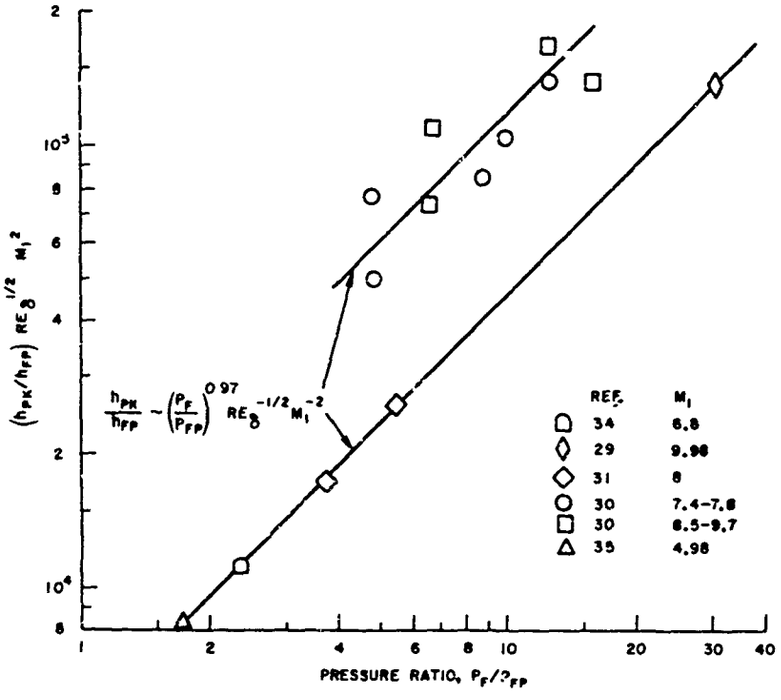

FIG. 27. Correlation of Peak Heat-Transfer Coefficient With Final Pressure, Mach Number, and Reynolds Number Based on Boundary-Layer Thickness for Laminar Boundary Layer.

These relations, particularly the latter, correlate the few data points other than those of Popinski extremely well. The Popinski data appear to follow the same slope but are translated upward, indicating higher heating rates. The slope of these data indicates a relation of the form

$$\frac{h_{PK}}{h_{FP}} \sim \left(\frac{P_F}{P_{FP}}\right)^{0.97} Re_\delta^{-1/2} M_1^{-2}$$

Turbulent Interactions

The correlations of peak turbulent heat-transfer coefficients with peak pressure and final pressure (Fig. 17 and 20, respectively) suggest that peak heat-transfer increases with increasing Mach number. The correlation of the form

$$\frac{h_{PK}}{h_{FP}} M_1^{-1} \quad \text{versus} \quad \frac{P_F}{P_{FP}}$$

was attempted to account for this effect. The results, shown in Fig. 28, indicate peak heat-transfer to be a weaker function of Mach number than that attempted, particularly at the higher Mach numbers.

Correlations of peak turbulent heat-transfer with Reynolds number based on both reference distance and boundary-layer thickness provide a slight improvement over the correlations with final pressure alone. Results of these correlations (Fig. 29 and 30) were used to develop the following two relations:

$$\frac{h_{PK}}{h_{FP}} = 28.2 \frac{\left(\frac{P_F}{P_{FP}}\right)^{0.74}}{Re_{x_{REF}}^{1/5}}$$

$$\frac{h_{PK}}{h_{FP}} = 12.2 \frac{\left(\frac{P_F}{P_{FP}}\right)^{0.71}}{Re_\delta^{1/5}}$$

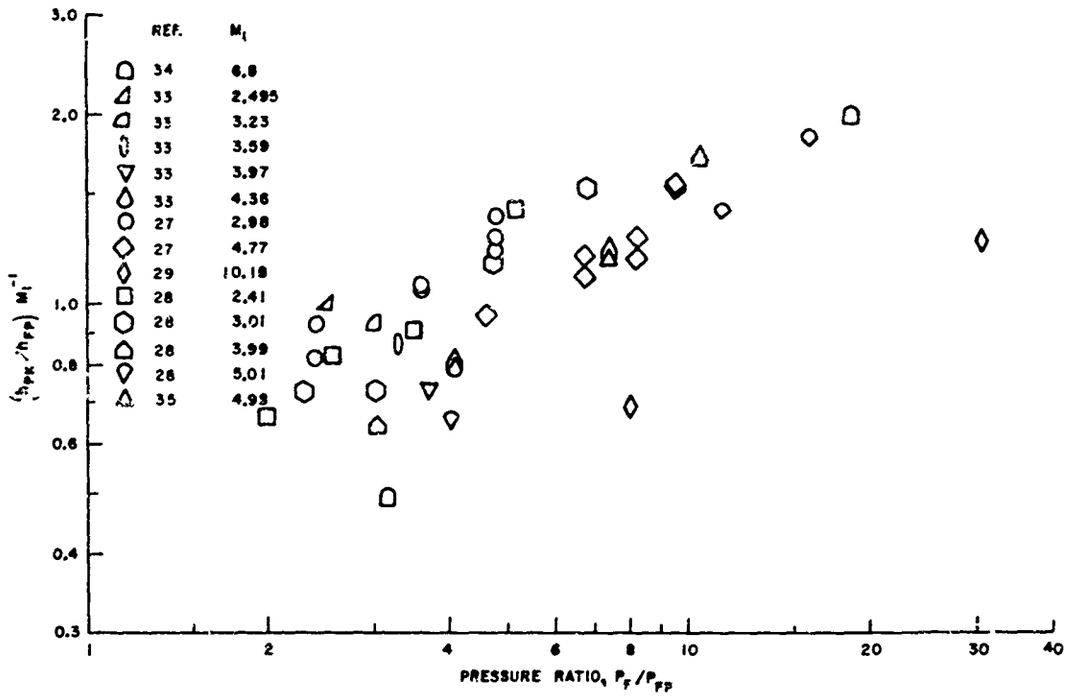

FIG. 28. Correlation of Peak Heat-Transfer Coefficient With Final Pressure and Mach Number for Turbulent Bourdary Layer.

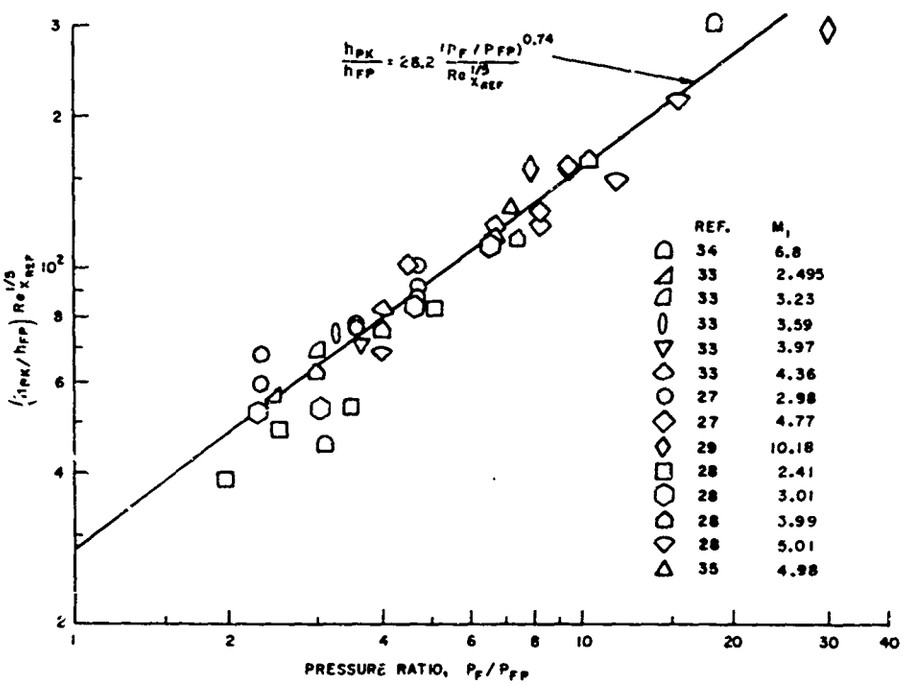

FIG. 29. Correlation of Peak Heat-Transfer Coefficient With Final Pressure and Reynolds Number for Turbulent Boundary Layer.

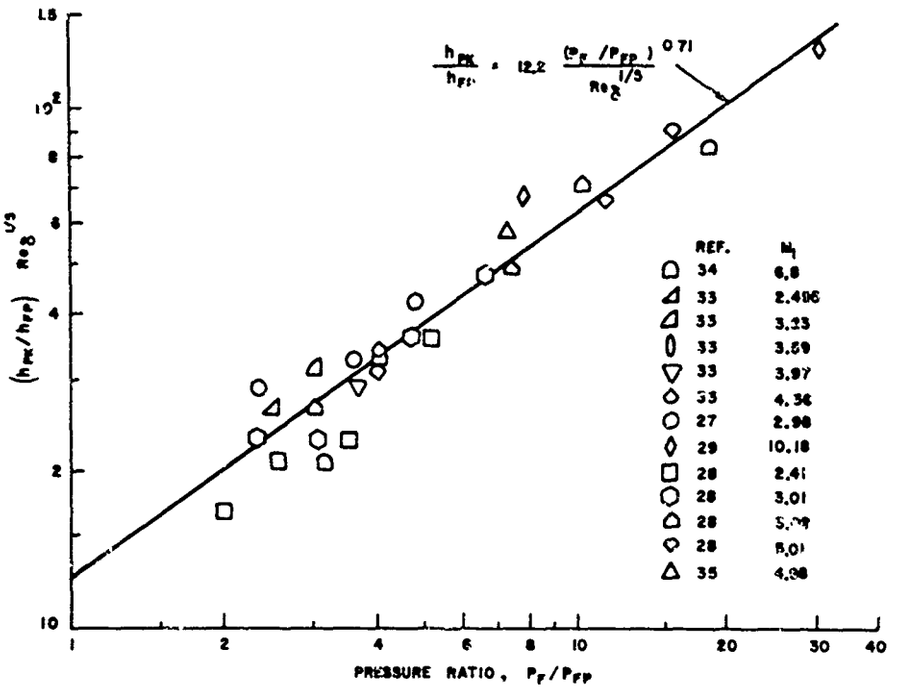

FIG. 30. Correlation of Peak Heat-Transfer Coefficient With Final Pressure and Reynolds Number Based on Boundary-Layer Thickness for Turbulent Boundary Layer.

Section 6
RESULTS

Results of the peak heat-transfer correlations indicate the following trends:

1. The increase in heat-transfer coefficient caused by shock wave-boundary layer interactions is greater in laminar interactions than that in turbulent interactions.

2. When transition occurs in the interaction region, the increase in heat-transfer coefficient is even greater. This is to be expected since in addition to the increased-heating rate caused by the shock interaction, the increased-heating rate associated with turbulent flow also exists.

Although the results of the correlations are not so successful as had been hoped, particularly in the case of laminar interactions, they can be used to provide a rapid preliminary estimate of the peak heat-transfer coefficient in shock wave-boundary layer interaction regions. For this purpose, the expressions relating peak heat-transfer to final pressure are the most useful of all developed because of their simplicity. The more involved correlations provided little improvement and, in some cases, were not so successful as the correlations with final pressure alone.

Possible explanations for the lack of success achieved in the peak heat-transfer correlations follow.

EXPERIMENTAL TECHNIQUES

Although all of the data used in the correlations came from wind tunnel investigations, in which test conditions may be carefully monitored, several variations in experimental techniques were involved. Some of the studies utilized separate models for measuring pressure and heat-transfer distributions so that these parameters could not be measured simultaneously. Correlations between pressure and heat transfer were thus affected by possible variations in flow condition

Although most of the studies did not state the overall accuracy of the data, several did mention difficulties encountered during testing. Experimental accuracies of 15 and 20% were given, and it is doubtful if any of the data are much more accurate than this. This could account for much of the scatter in the correlations.

Data were obtained for interactions on both hot and cold walls and under transient and steady-state conditions. The difference in heat-transfer measurement techniques and the various assumptions made in reducing the data to local heating rates, Stanton numbers, and heat-transfer coefficients added to the difficulty of comparing the results of various tests.

MEASUREMENT OF PEAK HEATING RATE

Because large gradients in heating rate exist in shock wave-boundary layer interaction regions, it is difficult to measure peaks in heating-rate distributions. When the spacing of sensors is not dense enough, it is possible to miss a measurement at or near the peak value.

METHOD OF PRESENTING DATA

Ideally, all of the heat-transfer data should be nondimensionalized by a common reference value, such as a theoretical heat-transfer coefficient calculated by a particular method. Unfortunately, because the published data were presented in a variety of ways, this was not possible. It was desired to reference all peak heat-transfer coefficients to the value that would exist at the reference point (Fig. 10) if the flow were undisturbed. Reference values included theoretical and experimental heat-transfer coefficients for undisturbed flow over flat plates, and experimental values upstream of the interaction. In most of the cases in which the latter value was used, the difference between the reference point and the beginning of the interaction region was small, compared to the distance from the beginning of the boundary layer. Consequently, the difference in heat-transfer coefficient at the two locations was also small.

In some cases, it was difficult to accurately determine the peak values of the pressure and heat-transfer distributions from the graphical forms used in presenting the data.

STATE OF THE BOUNDARY LAYER

A major cause for the poor correlations obtained with the laminar data might be the possibility of undetected transition in the interaction region. This could explain why the data of Popinski, in Fig. 26 and 27, are translated upward from the rest of the data points, which correlate quite well.

Another cause of scatter in the correlations might be the nature of separated flow, which makes it difficult to repeat results on successive test runs let alone to compare results obtained at different facilities.

Section 7

CONCLUSIONS AND RECOMMENDATIONS FOR FURTHER STUDY

CONCLUSIONS

1. Heating rates in shock wave-boundary layer interaction regions are significantly higher than the normally predicted values. These increases in heating rate are highest for cases in which transition occurs in the interaction region. Greater heating rate increases occur in laminar interactions than in turbulent interactions.

2. Sufficient experimental data are not available to allow the development of rapid empirical means for predicting the heat-transfer distribution in interaction regions. Correlations are made between peak experimental heating rates in interaction regions and various flowfield parameters with limited success.

3. Peak heat-transfer in turbulent interaction-regions may be estimated by the following relation that involves the inviscid pressure rise across the interaction:

$$\frac{h_{PK}}{h_{FP}} = \left(\frac{P_F}{P_{FP}}\right)^{0.85}$$

Peak heat-transfer data for laminar interactions do not correlate nearly so well as the turbulent data; the following expression is suggested for use in providing qualitative estimates only:

$$\frac{h_{PK}}{h_{FP}} = \left(\frac{P_F}{P_{FP}}\right)^{1.3}$$

Sufficient experimental data are not available for transitional interactions to allow development of empirical peak heat-transfer prediction techniques.

RECOMMENDATIONS FOR FURTHER STUDY

1. The geometry of shock wave-boundary layer interaction regions (interaction and separation lengths) should be further investigated to allow the development of general expressions for predicting heat-transfer distributions.

2. More experimental data are required—particularly for laminar and transitional interactions—so that more valid expressions for predicting peak heating rate may be developed. Extreme care should be taken in conducting laminar investigations to determine whether or not transition occurs in the interaction region.

3. Investigation of the boundary-layer thickness through the interaction region would provide a useful parameter for peak heat-transfer correlations.

4. Studies should be made to investigate heat-transfer distributions immediately downstream of interaction regions. This would be particularly useful for shock-impingement interactions.

Appendix

CALCULATION OF THEORETICAL INVISCID PRESSURE RATIO ACROSS SHOCK INTERACTION

The theoretical inviscid pressure ratio across a shock interaction may be calculated by using the applicable oblique (Ref. 46) or conical (Ref. 47) shock relations. These relations require that only the Mach number upstream of the interaction, M_1, and the flow deflection angle, θ, be known. In the case of a compression-corner interaction with separation, an improved estimate of the pressure ratio may be made by including Reynolds number effects.

If the upstream Mach number is not known, it may be calculated from the upstream pressure, free-stream pressure, and free-stream Mach number. The following procedure assumes an isentropic compression of a perfect gas ($\gamma = 1.4$) through a weak leading-edge disturbance:

$$\frac{P_\infty}{P_{T_\infty}} = \left(1 + \frac{M_\infty^2}{5}\right)^{-7/2}$$

$$\frac{P_1}{P_{T_1}} = \left(1 + \frac{M_1^2}{5}\right)^{-7/2}$$

$$P_{T_1} = P_{T_\infty} \text{ (Isentropic compression from } P_\infty \text{ to } P_1)$$

$$\frac{P_1}{P_\infty} = \left(\frac{1 + M_1^2/5}{1 + M_\infty^2/5}\right)^{-7/2}$$

$$M_1 = \left(5\left[\left(\frac{P_1}{P_\infty}\right)^{-2/7}\left(1 + \frac{M_\infty^2}{5}\right) - 1\right]\right)^{1/2}$$

The methods used to calculate inviscid pressure ratios, expressed as P_F/P_{FP} in the correlations given in Section 5, are described for the various configurations in the following text. Nomenclature refers to Fig. 10.

SHOCK IMPINGEMENT ON FLAT PLATE

The pressure ratio, P_F/P_{FP}, is calculated using the oblique shock relations:

$$\beta_1 = f(M_1 , \theta)$$

and is obtained by solving the following cubic equation:

$$\sin^6 \beta_1 + b \sin^4 \beta_1 + c \sin^2 \beta_1 + d = 0 \qquad (1)$$

where

$$b = - \frac{M_1^2 + 2}{M_1^2} - \gamma \sin^2 \theta$$

$$c = \frac{2 M_1^2 + 1}{M_1^4} + \left[\frac{(\gamma + 1)^2}{4} + \frac{\gamma - 1}{M_1^2} \right] \sin^2 \theta$$

$$d = - \frac{\cos^2 \theta}{M_1^4}$$

$$\frac{P_2}{P_1} = \frac{7 M_1^2 \sin^2 \beta_1 - 1}{6} = \xi_1 \qquad (2)$$

$$M_2 = \left[\frac{\xi_1 + 6}{7\,\xi_1 \sin^2\left(\beta_1 - \theta\right)}\right]^{1/2} \tag{3}$$

$$\beta_2 = f(M_2\ ,\ \theta) \qquad \text{(Ref. Eq. 1)}$$

$$\frac{P_3}{P_2} = \frac{7\,M_2^2 \sin^2 \beta_2 - 1}{6} = \xi_2 \tag{4}$$

$$M_3 = \left[\frac{\xi_2 + 6}{7\,\xi_2 \sin^2\left(\beta_2 - \theta\right)}\right] \tag{5}$$

$$\frac{P_F}{P_{FP}} = \frac{P_3}{P_1} = \left(\frac{P_2}{P_1}\right)\left(\frac{P_3}{P_2}\right) \tag{6}$$

SHOCK IMPINGEMENT ON CYLINDER

Calculations for conditions in Region 2 (β_1, P_2/P_1, M_2) are the same as those for impingement on a flat plate.

Conditions in Region 3 (β_3, P_3/P_2, M_3) are obtained from empirical conical shock relations (Ref. 47).

$$\beta_2 = \sin^{-1}\left\{\frac{1}{M_1^2} + \frac{1}{2}\left[G_2 + G_1 \sin^2\theta - \left\{\left[G_2 - G_1 \sin^2\theta\right]^2 - \left[\left(G_3 - G_1\right)\sin^2\theta\right]^2\right\}^{1/2}\right]\right\}^{1/2} \tag{7}$$

where

$$G_1 = \frac{\gamma + 1}{2}\ ,\quad G_2 = 1 - \frac{1}{M_2^2}\ ,\quad G_3 = \gamma\left(1 + \frac{1}{M_2^2}\right)$$

If $\theta \geq \sin^{-1} (G_2/G_3)^{1/2}$ in the above equations, the shock is detached, and a solution is not readily obtainable.

$$C_{P_{3_S}} = \frac{1}{2}\left[F_2 + F_1 \sin^2\theta - \left\{\left[F_2 - F_1 \sin^2\theta\right]^2 - \left[\left(F_3 - F_1\right)\sin^2\theta\right]^2\right\}^{1/2}\right] \tag{8}$$

where

$$F_1 = \frac{\gamma + 7}{4} - \left(\frac{\gamma - 1}{4}\right)^2 + \frac{6}{M_2^6} + \frac{M_2^2 - 1}{M_2^4 \sin\theta}$$

$$F_2 = \frac{1}{2}\left(\frac{\gamma + 7}{\gamma + 1}\right)\left(1 - \frac{1}{M_2^2}\right)\left(1 + \frac{1}{M_2^6}\right)$$

$$F_3 = \frac{\gamma}{2}\left(\frac{\gamma + 7}{\gamma + 1}\right)\left(1 + \frac{1}{M_2^2}\right)\left(1 + \frac{1}{M_2^6}\right)$$

$$\frac{P_{3S}}{P_2} = \left(C_{P_{3_S}} M_2^2 \frac{\gamma}{2}\right) + 1 \tag{9}$$

$$\frac{P_F}{P_{FP}} = \frac{P_{3S}}{P_1} = \left(\frac{P_{3S}}{P_2}\right)\left(\frac{P_2}{P_1}\right) \tag{10}$$

The Mach number on the surface of the cylinder, M_{3_S}, is obtained by assuming an isentropic compression from the pressure and the Mach number immediately behind the reflected conical shock, P_3 and M_3, to the pressure on the surface of the cylinder, P_{3_S}. From oblique shock relations P_3 and M_3 are calculated:

$$\frac{P_3}{P_2} = \frac{7\ M_2^2 \sin^2 \beta_2 - 1}{6} = \xi_2 \tag{11}$$

$$M_3 = \left[\frac{\xi_2 + 6}{7\ \xi_2 \sin^2 \left(\beta_2 - \theta\right)}\right]^{1/2}$$

$$M_{3_S} = \left\{5\left[\left(\frac{P_{3_S}}{P_2}\right)^{-2/7} \left(1 + \frac{M_3^2}{5}\right) - 1\right]\right\}^{1/2}$$

WEDGE COMPRESSION CORNER

Attached Boundary Layer

The calculation of β_1, P_2/P_1, and M_2 is the same as that for the case of shock impingement on a flat plate:

$$\frac{P_F}{P_{FP}} = \frac{P_2}{P_1}$$

Separated Boundary Layer

In the case of separated compression-corner flow, the overall pressure rise is assumed to take place by means of a double compression. The pressure behind the separation shock wave, P_2, is assumed to be identical with the plateau pressure, P_{PL}, and is obtained from the expressions

$$C_{P_{PL_{LAM}}} = 1.6 \left(Re_{x_{REF}}\right)^{-1/4} \left(M_1^2 - 1\right)^{-1/4} \tag{12}$$

$$C_{P_{PL_{TURB}}} = 1.7 \left(Re_{x_{REF}}\right)^{-1/10} \left(M_1^2 - 1\right)^{-1/4} \tag{13}$$

$$\frac{P_2}{P_1} = \frac{P_{PL}}{P_1} = \left(C_{P_{PL}}\ M_1^2\ \frac{\gamma}{2}\right) + 1 = \xi_1 \tag{14}$$

Equations 12 and 13 are taken from Ref. 43. The separation angle, θ', is calculated as being the deflection angie required to create the rise to the plateau pressure.

$$\theta' = \sin^{-1}\left(\frac{6\ \xi_1 + 1}{7\ M_1^2}\right)^{1/2} \tag{15}$$

$$M_2 = \left[\frac{M_1^2\ (6\ \xi_1 + 1) - 5\ (\xi_1^2 - 1)}{\xi_1\ (\xi_1 + 6)}\right]^{1/2} \tag{16}$$

$$\sin(\beta_1 - \theta') = \left(\frac{\xi_1 + 6}{7\ \xi_1\ M_2^2}\right)^{1/2} \tag{17}$$

$$\theta'' = \theta - \theta' \tag{18}$$

$$\beta_2 = f(M_2\ ,\ \theta'') \qquad \text{(Ref. Eq. 1)}$$

$$\frac{P_3}{P_2} = \frac{7\ M_2^2 \sin^2 \beta_2 - 1}{6} = \xi_2$$

$$M_3 = \left[\frac{\xi_2 + 6}{7\ \xi_2 \sin^2 (\beta_2 - \theta'')}\right]^{1/2}$$

$$\frac{P_F}{P_{FP}} = \frac{P_3}{P_1} = \left(\frac{P_3}{P_2}\right)\left(\frac{P_2}{P_1}\right)$$

CONICAL FLARE COMPRESSION-CORNER

Attached Boundary Layer

Conditions in Region 2 (β_2, P_2/P_1, P_{2_S}, M_2, and M_{2_S}) are calculated by using the same equations as those used for shock reflection from a cylinder.

$$\beta_1 = f(M_1 , \theta) \qquad \text{(Ref. Eq. 7)}$$

$$\frac{P_{2_S}}{P_1} = f(M_1 , \theta) \qquad \text{(Ref. Eq. 8 and 9)}$$

$$\frac{P_2}{P_1} = f(M_1 , \beta_1) \qquad \text{(Ref. Eq. 2)}$$

$$M_2 = f(\beta_1 , \theta) \qquad \text{(Ref. Eq. 3)}$$

$$M_{2_S} = f\left(\frac{P_{2_S}}{P_2} , M_2\right) \qquad \text{(Ref. Eq. 11)}$$

$$\frac{P_F}{P_{FP}} = \frac{P_{2_S}}{P_1} \qquad (19)$$

Separated Boundary Layer

The ideal method of calculating the separation angle, θ', would be to assume that P_{2_S}/P_1 is equal to P_{PL}/P_1, to calculate P_{PL}/P_1 from Eq. 12 or 13, and to calculate θ' from Eq. 8. Because there is difficulty in solving Eq. 8 for θ', the overall pressure rise may be approximated by assuming that $\theta' = \theta'' = \theta/2$. The procedure for calculating P_F/P_{FP} then becomes

$$\beta_1 = f(M_1 , \theta') \qquad \text{(Ref. Eq. 7)}$$

$$C_{P_{2_S}} = f(M_1 , \theta') \qquad \text{(Ref. Eq. 8)}$$

$$\frac{P_{2_S}}{P_1} = f\left(C_{P_{2_S}} , M_1\right) \qquad \text{(Ref. Eq. 9)}$$

$$\frac{P_2}{P_1} = f(M_1 , \beta_1) \qquad \text{(Ref. Eq. 2)}$$

$$M_2 = f(\beta_1 , \theta') \qquad \text{(Ref. Eq. 3)}$$

$$M_{2_S} = f\left(\frac{P_{2_S}}{P_2} , M_2\right) \qquad \text{(Ref. Eq. 11)}$$

$$\beta_2 = f\left(M_{2_S} , \theta''\right) \qquad \text{(Ref. Eq. 7)}$$

$$C_{P_{3_S}} = f\left(M_{2_S} , \theta''\right) \qquad \text{(Ref. Eq. 8)}$$

$$\frac{P_{3_S}}{P_{2_S}} = f\left(C_{P_{3_S}} , M_{2_S}\right) \qquad \text{(Ref. Eq. 9)}$$

$$\frac{P_3}{P_2} = f\left(M_{2_S} , \beta_2\right) \qquad \text{(Ref. Eq. 2)}$$

$$M_3 = f(\beta_2 , \theta'') \qquad \text{(Ref. Eq. 3)}$$

$$M_{3_S} = f\left(\frac{P_{3_S}}{P_3}\ ,\ M_3\right) \qquad \text{(Ref. Eq. 11)}$$

$$\frac{P_F}{P_{FP}} = \frac{P_{3_S}}{P_1} = \left(\frac{P_{3_S}}{P_{2_S}}\right)\left(\frac{P_{2_S}}{P_1}\right) \qquad (20)$$

FIN SHOCK

The calculation of β_2, P_2/P_1, and M_2 is the same as that for shock impingement on a flat plate.

$$\frac{P_F}{P_{FP}} = \frac{P_2}{P_1}$$

METHODS OF SOLUTION

Graphical solutions are available for all of the previously mentioned parameters (Ref. 46). The large number of data points involved in the correlations, however, made graphical solutions impractical. For this reason, a FORTRAN IV computer program was written for the UNIVAC 1108 computer to solve the inviscid flow equations.

REFERENCES

1. Naval Missile Center. "Aircraft-Missile Interference Effects," by C. F. Markarian, and C. M. Martin; published in Proceedings of the Seventh U. S. Navy Symposium on Aeroballistics (BOWACA), held at Point Mugu, 7-9 June 1966. Point Mugu, Calif., NMC, June 1966. (NMC-MP 66-10.)

2. Bertram, Mitchell H., and M. Margarette Wiggs. "Effect of Surface Distortions on the Heat Transfer to a Wing at Hypersonic Speeds," AIAA J, Vol. 1 (June 1963), pp. 1313-19.

3. Datis, Angelo, B. G. Broach, and H. H. Yen. "Heat Transfer in the Vicinity of Two-Dimensional Protuberances," J SPACECRAFT ROCKETS, Vol. 1 (November-December 1964), pp. 678-80.

4. General Dynamics. Turbulent Flow and Heat Transfer Near Surface Protuberances, by H. Dershin. Pomona, Calif., GD, December 1963. (TM No. 6-349-127.)

5. North American Aviation, Inc. Aerodynamic Heating in the Vicinity of Surface Protuberances, by Michael C. Fong. Columbus, Ohio, NAAI, 3 March 1966. (NA 65H-891.)

6. Surber, True E. "Heat Transfer in the Vicinity of Surface Protuberances," J SPACECRAFT ROCKETS, Vol. 2 (November-December 1965), pp. 978-80.

7. Truitt, Robert W. "Hypersonic Turbulent Boundary-Layer Interference Heat Transfer in Vicinity of Protuberances," AIAA J, Vol. 3 (September 1965), pp. 1754-55.

8. National Aeronautics and Space Administration. Turbulent Heat-Transfer Coefficients in the Vicinity of Surface Protuberances, by Richard J. Wisniewski. Washington, D. C., NASA, October 1958. (NASA Memo 10-1-58E.)

9. -----. Interference Heating on a Swept Cylinder in Region of Interaction With a Wedge at Mach Number 8, by Dennis M. Bushnell. Washington, D. C., NASA, December 1965. (NASA TN-D-3094.)

10. Air Force Flight Dynamics Laboratory. Heating in Regions of Interfering Flow Fields: Part II. Leading Edge Shock Impingement, by C. F. Gulloran and others. Wright-Patterson Air Force Base, Dayton, Ohio, AFFDL/AFSC, January 1967. (AFFDL-TR-65-49, Part II.)

11. Arnold Engineering Development Center. Measurements of Shock-Impingement Effects on the Heat-Transfer and Pressure Distributions on a Hemi-Cylindrical Model at Mach Number 19, by E. C. Knox. Arnold Air Force Base, Tenn., AEDC/AFSC, November 1965. (AEDC-TR-65-245.)

12. Air Force Office of Scientific Research. Hypersonic Flow Along Two Intersecting Planes, by Robert J. Cresci, Polytechnic Institute of Brooklyn. Arlington, Va., AFOSR/PIB, March 1966. (AFOSR Report 66-0500.)

13. Dorrance, William H. Viscous Hypersonic Flow. New York, McGraw-Hill, 1962. Chap. 6.

14. National Aeronautics and Space Administration. Semiempirical Method for Predicting Effects of Incident-Reflecting Shocks on the Turbulent Boundary Layer, by S. Z. Pinckney. Washington, D. C., NASA, October 1965. (NASA TN D-3029.)

15. Curle, N. "The Effects of Heat Transfer on Laminar-Boundary Layer Separation in Supersonic Flow." AERON QUART, Vol. XII (November 1961), pp. 309-36.

16. North Atlantic Treaty Organization: Advisory Group for Aeronautical Research and Development. Boundary Layer Separation in the Presence of Heat Transfer, by G. E. Gadd, paper presented at the Boundary Layer Research Meeting of AGARD Fluid Dynamics Panel, London, England, NATO/AGARD, 25-29 April 1960. (AGARD Report 280.)

17. Aeronautical Systems Division. Supersonic Flow About General Three-Dimensional Blunt Bodies: Vol. II. Heat Transfer Due to the Interaction between a Swept Planar Shock Wave and a Laminar Boundary Layer, by A. Martellucci and P. A. Libby. Wright-Patterson Air Force Base, Dayton, Ohio, ASD/AFSC, October 1962. (ASD-TR-61-727, Vol. II.)

18. Crocco, L., and L. Lees. "A Mixing Theory for the Interaction Between Dissipative Flows and Nearly Isentropic Streams," J AERON SCI, Vol. 19 (October 1952), pp. 649-76.

19. Glick, Herbert S. "Modified Crocco-Lees Mixing Theory for Supersonic Separated and Reattaching Flows," J AEROSPACE SCI, Vol. 29 (October 1962), pp. 1238-44.

20. Tani, Itiro. "On the Approximate Solution of the Laminar Boundary Layer Equations," J AERON SCI, Vol. 21 (July 1954), pp. 487-504.

21. Lees, Lester, and Barry L. Reeves. "Supersonic Separated and Reattaching Laminar Flows: I. General Theory and Application to Adiabatic Boundary-Layer/Shock-Wave Interactions," AIAA J, Vol. 2 (November 1964), pp. 1907-1920.

22. Cornell Aeronautical Laboratory, Inc. An Analytical Study of Separated Flows Induced by Shock Wave-Boundary Layer Interaction, by M. S. Holden, for Goddard Space Flight Center. Buffalo, N. Y., CAL/GSFC, December 1963. (CAL Report No. AI-1972-A-3.)

23. Makofski, R. A. "A Two-Parameter Method for Shock Wave-Laminar Boundary Layer Interaction and Flow Separation," in Proceedings of the 1963 Heat Transfer and Fluid Mechanics Institute. Stanford, Calif., Stanford University Press, 1963. Pp. 112-37.

24. Air Force Flight Dynamics Laboratory. Calculations of Laminar Separation With Free Interaction by the Method of Integral Relations, by Jack N. Nielsen, Larry L. Lynes, and Frederick K. Goodwin. Wright-Patterson Air Force Base, Dayton, Ohio, AFFDL/AFSC, January 1966. (Technical Report AFFDL-TR-65-107.)

25. National Advisory Committee for Aeronautics. Investigation of Separated Flows in Supersonic and Subsonic Streams With Emphasis on the Effect of Transition, by Dean R. Chapman, Donald M. Kuehn, and Howard K. Larson. Washington, D. C., 1958, NACA. (NACA Report 1356.)

26. National Aeronautics and Space Administration. The Interaction of an Oblique Shock Wave With a Laminar Boundary Layer, by R. J. Hakkinen, I. Greber, L. Trilling, and S. S. Abarbanel. Washington, D. C., NASA, March 1959. (NASA Memorandum 2-18-59W.)

27. North American Aviation, Inc. Thermal Effects of Shock Wave Turbulent Boundary Layer Interaction at Mach Numbers 3 and 5, by V. Levin and T. J. Fabish. Columbus, Ohio, NAAI, 12 November 1962. (NA 62H-795.)

28. Douglas Aircraft Company. Heat Transfer in Shock Wave-Turbulent Boundary Layer Interaction Regions, by S. Sayano. Santa Monica, Calif., DAC, 19 November 1962. (Douglas Report SM-42567.)

29. Arnold Engineering Development Center. Investigation of Flow Field Interference Caused by Shock Impingement on a Flat Plate at Mach Numbers of 6, 8, and 10, by J. D. Magnan, Jr. and C. J. Spurlin. Arnold Air Force Base, Tenn., AEDC/AFSC, April 1966. (AEDC-TR-66-85.)

30. Lockheed-California Company. Shock Wave-Boundary Layer Interaction, by Zenon Popinski. Burbank, Calif., LCC, 29 June 1965. (Report LR 18307.)

31. Needham, David A. "A Heat Transfer Criterion for the Detection of Incipient Separation in Hypersonic Flow." AIAA J, Vol. 3 (April 1965), pp. 781-83.

32. Shumway, Rex W. Heat Transfer in Shock Boundary Layer Interaction Regions. (M. S. in Mechanical Engineering) Brigham Young University, Provo, Utah, August 1965.

33. Royal Aircraft Establishment. Heat Transfer in the Vicinity of a 15° Compression Corner at Ma Numbers From 2.5 to 4.4, by R. C. Hastings and others. Great Britian, RAE, June 1966. (Technical Report No. 66171.)

34. National Aeronautics and Space Administration. Heat Transfer and Pressure Distribution at a Mach Number of 6.8 on Bodies With Conical Flares and Extensive Flow Separation, by John V. Becker and Peter F. Korycinski. Washington, D. C., NASA, April 1962. (NASA TN D-1260.)

35. Schaeffer, John W., and Harold Ferguson. "Investigation of Separation and Associated Heat Transfer and Pressure Distribution on Cone-Cylinder-Flare Configuration at Mach Five." ARS J, Vol. 32 (May 1962), pp. 762-70.

36. Air Force Flight Dynamics Laboratory. Heating in Regions of Interfering Flow Fields: Part I. Two- and Three-Dimensional Laminar Interactions at Mach 8, by C. E. Gulbran and others. Wright-Patterson Air Force Base, Dayton, Ohio, AFFDL/AFSC, 23 July 1965. (AFFDL TR 65-49, Part I.)

37. Miller, D. S., and others. "A Study of Shock Impingement on Boundary Layers at Mach 16," in Proceedings of the 1962 Heat Transfer and Fluid Mechanics Institute. Stanford, Calif., Stanford University Press, 1962. Pp. 255-78.

38. National Aeronautics and Space Administration. Measurement of Aerodynamic Heat Transfer to a Deflected Trailing-Edge Flap on a Delta Fin in Free Flight at Mach Numbers From 1.5 to 2.6, by Leo T. Chauvin and James J. Buglia. Washington, D. C., NASA, 1957. (NASA TN D-250.)

39. -------. Measurements of Aerodynamic Heat Transfer on a 15° Cone-Cylinder-Flare Configuration in Free Flight at Mach Numbers up to 4.7, by Charles B. Rumsey and Dorothy B. Lee. Washington, D. C., NASA, May 1961. (NASA TN D-824.)

40. Erdos, John, and Adrian Pallone. "Shock-Boundary Layer Interaction and Flow Separation," in Proceedings of the 1962 Heat Transfer and Fluid Mechanics Institute. Stanford, Calif., Stanford University Press, 1962. Pp. 239-54.

41. National Aeronautics and Space Administration. Analysis of Hypersonic Pressure and Heat Transfer Tests on a Flat Plate With Flap and a Delta Wing With Body, Elevons, Fins, and Rudders, by H. L. Giles and J. W. Thomas. Washington, D. C., NASA, August 1966. (NASA CR-536.)

42. Kreith, Frank. Principles of Heat Transfer. Scranton, N. J., International, 1963. Chap. 6.

43. Douglas Aircraft Company. Flow Separation in High Speed Flight, A Review of the State-Of-The Art, by J. E. Wuerer and F. I. Clayton. Santa Monica, Calif., DAC, April 1965. (Douglas Report SM-46429.)

44. Princeton University. The Peak Pressure Rise Across an Oblique Shock Emerging From a Turbulent Boundary Layer Over a Plane Surface, by L. Crocco and R. F. Probstein, Princeton, N. J., PU, March 1954. (Report 254.)

45. National Advisory Committee for Aeronautics. Pressure Rise Associated With Shock-Induced Boundary-Layer Separation, by Eugene S. Love, Washington, D. C., NACA, December 1955. (NACA Technical Note 3601.)

46. National Advisory Committee for Aeronautics. Equations, Tables, and Charts for Compressible Flow, by Ames Research Staff, Washington, D. C., NACA/AR, 1953. (Report 1135.)

47. Simon, Wayne E., and Louise A. Walter. "Approximations for Supersonic Flow Over Cones." AIAA J, Vol. 1 (July 1963), pp. 1696-98.

48. National Advisory Committee for Aeronautics. A Theoretical Analysis of Heat Transfer in Regions of Separated Flow, by Dean R. Chapman, Washington, D. C., NACA, October 1956. (NACA TN-3792.)

49. Larson, Howard K. "Heat Transfer in Separated Flows," J AEROSPACE SCI, Vol. 26 (November 1959), pp. 731-38.

50. Miller, D. S., R. Hijman and M. E. Childs. "Mach 8 to 22 Studies of Flow Separations Due to Deflected Control Surfaces," AIAA J, Vol. 2 (February 1964), pp. 312-21.

51. Sterrett, J. R., and P. F. Holloway. "On the Effect of Transition on Parameters Within a Separation Region at Hypersonic Speeds—With Emphasis on Heat Transfer," presented at the Fluids Engineering Division Conference Symposium on Fully Separated Flows, Philadelphia, Pa., 18-20 May 1964, J HEAT TRANSFER (ASME, Trans), pp. 15-26.

52. National Aeronautics and Space Administration. An Investigation of Heat Transfer Within Regions of Separated Flow at a Mach Number of 6.0, by P. F. Holloway, J. R. Sterrett, and H. S. Creekmore. Washington, D. C., NASA, November 1965. (NASA TN D-3074.)

53. Spalding, D. B. "Heat Transfer From Turbulent Separated Flows," J FLUID MECH, Vol. 27 (11 January 1967), pp. 97-109.

BIBLIOGRAPHY

1. Aerospace Research Laboratory: Office of Aerospace Research. Theoretical and Experimental Studies of Laminar Flow Separation on Flat Plate-Wedge Compression Surfaces in the Hypersonic Strong Interaction Regime, by M. S. Holden of Cornell Aeronautical Laboratory, Inc. Wright-Patterson Air Force Base, Dayton, Ohio, ARL/AFSC, May 1967. (ARL 67-9112.)

2. Air Force Flight Dynamics Laboratory. Heating in Regions of Interfering Flow Fields: Part III. Two-Dimensional Interaction Caused by Plane Shocks Impinging on Flat Plate Boundary Layers, by C. E. Gulbran and others. Wright-Patterson Air Force Base, Ohio, AFFDL/AFSC, March 1967. (AFFDL-TR-65-49, Part III.)

3. ------. Investigation of Hypersonic Inlet Shock Wave-Boundary Layer Interaction, by Paul H. Kutschenreuter, Jr., and others. Wright-Patterson Air Force Base, Ohio, AFFDL/AFSC, March 1965. (AFFDL-TR-65-36.)

4. Air Force Office of Scientific Research: Office of Aerospace Research: Air Force European Office of Research. Laminar Separation in Supersonic and Hypersonic Flows, by Jean J. Ginoux, of von Karman Institute for Fluid Dynamics, Rhode-Saint-Genese, Belgium. Arlington, Va., AFOSR/OAR/AFEOR, October 1965. (AF EOAR 65-11.)

5. ------. Supersonic Flow Over Flaps With Uniform Heat Transfer, by Jean J. Ginoux of von Karman Institute for Fluid Dynamics of Rhode-Saint-Genese, Belgium, Arlington, Va., AFOSR/OAR/AFEOR, September 1966. (Technical Note 30.)

6. Chilcott, R. E. "A Review of Separated and Reattaching Flows With Heat Transfer." INT J HEAT AND MASS TRANSFER, Vol. 10 (June 1967), pp. 783-97.

7. Cornell Aeronautical Laboratory. Separated Flow Studies of Hypersonic Speeds: Part II, Two-Dimensional Wedge Separated Flow Studies, by M. S. Holden, for Chief of Naval Research. Buffalo, N. Y., December 1964. (CAL Report AF-1285-A-13(2).)

8. Gadd, G. E. "A Theoretical Investigation of Laminar Separation in Supersonic Flow," J AERON SCI, Vol. 24 (October 1957), pp. 759-71.

9. Hankey, Wilbur L., and Ernest J. Cross. "Approximate Closed-Form Solution for Supersonic Laminar Separated Flows." AIAA J, Vol. 5 (April 1967), pp. 651-54.

10. National Aeronautical and Space Administration. Effect of Shock Impingement on the Distribution of Heat-Transfer Coefficients on a Right Circular Cylinder at Mach Numbers of 2.65, 3.51, and 4.44, by Robert A. Newlander. Washington, D. C., NASA, January 1961. (NASA TN D-642.)

11. National Aeronautics and Space Administration. Effects of Shock Wave Impingement on the Heat Transfer on a Cylindrical Leading Edge, by R. S. Hiers and W. J. Loubsky. Washington, D. C., NASA, February 1967. (NASA TN D-3859.)

12. Schlichting, Herman. Boundary Layer Theory, 2nd ed. New York, McGraw-Hill, 1963. Ch XV.

13. Shapiro, Ascher H. The Dynamics and Thermodynamics of Compressible Fluid Flow. New York, Ronald, 1954. Vol. 2, Ch. 28.

AUTHOR INDEX

REFERENCES

BIBLIOGRAPHY

Chilcott, R. E. 6
Cross, Ernest J. 9

Gadd, G. E. 8
Ginoux, Jean J. 4
Ginoux, J. J. 5
Gulbran, C. E., and others 2

Hankey, Wilbur L. 9
Heirs, R. S. 11
Holden, M. S. 1, 7

Kutschenreuter, Paul H., Jr., and others 3

Loubsky, W. J. 11

Newlander, Robert A. 10

Schlichting, Herman 12
Shapiro, Ascher H. 13

UNCLASSIFIED

Security Classification

DOCUMENT CONTROL DATA - R & D

Security classification of title, body of abstract and indexing annotation must be entered when the overall report is classified)

1 ORIGINATING ACTIVITY (Corporate author) Naval Weapons Center China Lake, California 93555	2a. REPORT SECURITY CLASSIFICATION UNCLASSIFIED 2b GROUP ---

3 REPORT TITLE

HEAT TRANSFER IN SHOCK WAVE-BOUNDARY LAYER INTERACTION REGIONS (U)

4 DESCRIPTIVE NOTES (Type of report and inclusive dates)

Aerodynamic heating, and literature search (FY 1967 and 1968)

5 AUTHOR(S) (First name, middle initial, last name)

C. Franklyn Markarian

6 REPORT DATE November 1968	7a. TOTAL NO OF PAGES 80	7b NO OF REFS 66
8a CONTRACT OR GRANT NO b PROJECT NO AIR-320-039/216-1/F009-10-01 c d	9a. ORIGINATOR'S REPORT NUMBER(S) NWC TP 4485 9b OTHER REPORT NO(S) (Any other numbers that may be assigned this report) None	

10 DISTRIBUTION STATEMENT

THIS DOCUMENT IS SUBJECT TO SPECIAL EXPORT CONTROLS AND EACH TRANSMITTAL TO FOREIGN GOVERNMENTS OR FOREIGN NATIONALS MAY BE MADE ONLY WITH PRIOR APPROVAL OF THE NAVAL WEAPONS CENTER.

11 SUPPLEMENTARY NOTES	12 SPONSORING MILITARY ACTIVITY Naval Air Systems Command Naval Material Command Washington, D. C. 20360

13 ABSTRACT

ABSTRACT. An investigation of the effect of shock wave-boundary layer interaction on aerodynamic heat-transfer coefficients is reported. A literature survey and empirical expressions for predicting peak heat-transfer coefficients in interaction regions, developed with the use of existing experimental data, are presented.

DD FORM 1 NOV 65 1473 (PAGE 1)

S/N 0101-807-6801

UNCLASSIFIED

Security Classification

14 KEY WORDS	LINK A		LINK B		LINK C	
	ROLE	WT	ROLE	WT	ROLE	WT
Aerodynamic heating Shock wave impingement Boundary-layer separation Pressure distributions						